UNIVERSIDADE FEDERAL DE PERNAMBUCO
CENTRO DE CIÊNCIAS EXATAS E DA NATUREZA
PHYSICS GRADUATE PROGRAM

Anderson de Souza Bibiano Filho

Kosterlitz-Thouless transition in a mixed-spin ladder under a magnetic field

Recife

2022

Anderson de Souza Bibiano Filho

Kosterlitz-Thouless transition in a mixed-spin ladder under a magnetic field

Dissertation presented to the graduate program in physics of the Physics Department at Universidade Federal de Pernambuco as a partial requirement to obtain a Master's degree in Physics.

Concentration area: Theoretical and Computational Physics

Supervisor: Renê Rodrigues Montenegro Filho

Recife

2022

Catalogação na fonte
Bibliotecária Nataly Soares Leite Moro, CRB4-1722

B581k Bibiano Filho, Anderson de Souza
Kosterlitz-Thouless transition in a mixed-spin ladder under a magnetic field / Anderson de Souza Bibiano Filho. – 2022.
96 f.: il., fig.

Orientador: Renê Rodrigues Montenegro Filho.
Dissertação (Mestrado) – Universidade Federal de Pernambuco. CCEN, Física, Recife, 2022.
Inclui referências.

1. Física da matéria condensada e de materiais. 2. Transições de fase quântica. 3. Modelo do Hamiltoniano de Heisenberg. I. Montenegro Filho, Renê Rodrigues (orientador). II. Título.

530.41 CDD (23. ed.) UFPE- CCEN 2023 - 37

ANDERSON DE SOUZA BIBIANO FILHO

KOSTERLITZ-THOULESS TRANSITION IN A MIXED-SPIN LADDER UNDER A MAGNETIC FIELD

Dissertação apresentada ao Programa de Pós-Graduação em Física da Universidade Federal de Pernambuco, como requisito parcial para a obtenção do título de Mestre em Física.

Aprovada em: 20/12/2022.

BANCA EXAMINADORA

_____

Prof. Renê Rodrigues Montenegro Filho
Orientador
Universidade Federal de Pernambuco

_____

Prof. Maurício Domingues Coutinho Filho
Examinador Interno
Universidade Federal de Pernambuco

_____

Prof. Natanael de Carvalho Costa
Examinador Externo
Universidade Federal do Rio de Janeiro

Dedico este trabalho a todos que me acompanharam até aqui, sejam professores, amigos, colegas, e, especialmente, família.

AGRADECIMENTOS

Inicio agradecendo meu professor orientador, Renê Montenegro, por toda paciência e recepção ao longo dos anos de iniciação científica e projeto de mestrado, indicando referências, orientando a pesquisa e texto de dissertação. Agradeço também Letícia Melo, que além dos auxilios prestados para a escrita do texto em inglês, se apresentou como uma grande companheira e parceira, fornecendo apoio e carinho durante todo meu mestrado. Agradeço meus amigos, em especial Naudson Lopes, Ruben Esteche e Pollyanna Alencar, meus colegas de curso, cuja companhia se mostrou essencial na minha jornada. Agradeço também a todos aqueles que, de alguma forma, contribuiram e prestigiaram meu trabalho. Por último, gostaria de reservar um agradecimento especial aos meus pais, Marta e Anderson Bibiano, e minha irmã, Juliana Bibiano, que forneceram toda a estrutura durante toda minha formação.

ABSTRACT

At zero temperature, thermal fluctuation is eliminated and phase transitions will occur due to quantum fluctuations that arise from the Heisenberg uncertainty principle. Magnetic insulators, described by the Heisenberg model Hamiltonian, are a known class of physical systems that can undergo quantum phase transitions when submitted to a magnetic field. The magnetic field induces the transition by closing energy gaps through the Zeeman effect. Examples of systems that undergo these transitions are the antiferromagnetic spin-1 chain, the antiferromagnetic spin-$\frac{1}{2}$ ladder, the ferrimagnetic mixed spin-1 and spin-$\frac{1}{2}$ chains and ladders. The presence of a gap in the energy spectrum with zero magnetic field leads to a magnetization plateau in the magnetization curve. We use the density matrix renormalization group to investigate the magnetization curves of the mixed spin-1 and spin-$\frac{1}{2}$ ladder, for antiferromagnetic and ferromagnetic couplings between the ladder legs $J_\perp$. For $J_\perp > 0$, the ground-state is ferrimagnetic with the total spin equal to $\frac{1}{3}$ of the saturation value, in accord with the Lieb-Mattis theorem. The magnetization curve presents a plateau at total magnetization $\frac{1}{3}$ of the saturation value, the $\frac{1}{3}$-plateau since the ground state has a gap to excitations that increase the total spin by 1 unit. Decreasing $J_\perp$ below zero, the ground state becomes a singlet, but the $\frac{1}{3}$-plateau survives down to a critical value $J_\perp = J_c$. Given that the gap closes with the magnetization fixed, it is a Kosterlitz-Thouless transition type. To determine J_c, we have made a finite-size scale analysis of the plateau width.

Keywords: quantum phase transitions; Heisenberg model Hamiltonian; mixed spin-1 and spin-$\frac{1}{2}$ ladder.

RESUMO

Em temperatura zero, flutuação térmica é eliminada e transições de fase irão ocorrer devido à flutuações que surgem do princípio da incerteza de Heisenberg. Isolantes magnéticos, descritos pelo modelo do Hamiltoniano de Heisenberg, são uma conhecida classe de sistemas que podem ser submetidos a transições de fase quântica quando expostos a um campo magnético. O campo magnético induz a transição fechando gaps de energia através do efeito Zeeman. Exemplos de sistemas que passam por essas transições são a cadeia antiferromagnética de spin-1, a cadeia escada antiferromagnética de spin-$\frac{1}{2}$, a cadeia ferrimagnética e a cadeia escada ferrimagnética de spin misturado com spin-1 e spin-$\frac{1}{2}$. A presença do gap no espectro de energia com campo magnético zero leva a um plateau de magnetização na curva de magnetização. Usamos o grupo de renormalização da matriz densidade para investigar curvas de magnetização da cadeia escada de spin misturado com spin-1 e spin-$\frac{1}{2}$, para acoplamento antiferromagnético e ferromagnético entre as pernas da escada $J_\perp$. Para $J_\perp > 0$, o estado fundamental é ferrimagnético com spin total igual a $\frac{1}{3}$ do valor de saturação, o $\frac{1}{3}$-plateau dado que o estado fundamental possui um gap para excitações que aumentam o spin total em 1 unidade. Diminuindo $J_\perp$ abaixo de zero, o estado fundamental se torna um singleto, mas o $\frac{1}{3}$-plateau sobrevive até o valor crítico $J_\perp = J_c$. Dado que o gap fecha sob magnetização constante, é uma transição do tipo Kosterlitz-Thouless. Para determinar J_c, fizemos análise de escala finita da largura do plateau.

Palavras-chaves: transições de fase quântica; modelo do Hamiltoniano de Heisenberg; cadeia escada de spin misturado com spin-1 e spin-$\frac{1}{2}$.

LIST OF FIGURES

CONTENTS

1 INTRODUCTION

Phase transitions are well-known phenomena in nature, displaying a fundamental and abundant role throughout physical research, ranging from the more popular examples such as the water phase transitions (usually found in textbooks) to more specific ones like the Kosterlitz-Thouless transition.

Temperature (T) is commonly found to be an important parameter for transitions on many physical systems: it can determine the physical states of water (solid, liquid, gaseous); it is fundamental for the operation of enzymes, a phenomenon known as enzyme temperature dependence (PINNEY et al., 2021); it determines conductivity properties of conductors (OHKAWA, 1978) and semiconductors (O'DONNELL; CHEN, 1991), ensuring that electrical devices will perform properly. These types of transitions that are determined by temperature occur due to thermal fluctuations. Pressure (P) is another parameter commonly referred to as an inducer of phase transitions, as it can determine the physical state of a variety of substances.

Magnetic field ($\vec{B}$) is also a parameter that can induce phase transition in magnetic materials. Magnetic dipoles have a tendency to align with the magnetic field. As B grows, so does the magnetization in the direction of $\vec{B}$, up to a saturation limit. The interaction between the magnetic field and magnetic moments in the system is usually expressed through the Zeeman term. Magnetic systems' phase transitions are described using interacting models, two important models being the Heisenberg and Ising models.

1.1 ISING AND HEISENBERG MODEL

One of the models that introduced phase transitions for magnetic systems was the Ising model (KOBE, 2000). It presents a formula to evaluate a magnetic system's energy for a given configuration of its magnetic dipoles, describing a magnetic system as a lattice with a distribution of interacting spins. In the Ising model, the interaction occurs between the z component of spin S_i^z. It predicts phase transitions from ordered to disordered states in both antiferromagnetic and ferromagnetic materials by either varying the applied magnetic field or the temperature. The model is known to have exact solutions. The first exact solution obtained for the model treated a one-dimensional chain and it presented no phase transition: correlation between sites spin decays exponentially and there is no long-range order between spins for

$T > 0$. An analytical solution for the two-dimensional lattice was obtained later by Onsager in a zero magnetic field. It exhibits a continuous phase transition from ordered to disordered phases by varying the temperature for the ferromagnetic case. At low temperatures ($T < T_c$, with T_c the critical temperature), ferromagnetic order is expected and magnetization will be non-null. Increasing temperature, the magnetization will continuously drop from the saturation value (at low temperature) to zero (above critical temperature).

Although the exact solutions were obtained for one and two dimensions, a solution of the Ising model in a three-dimensional lattice was never obtained. Analytical solutions for the Ising model are not easy to come by. An alternative is to use numerical approaches to simulate Ising model systems. The numerical alternative consists in using the Monte Carlo method through the Metropolis algorithm (FRICKE, 2006) to plot the magnetization curve as a function of temperature. For the ferromagnetic case, the algorithm provides the result of a decreasing magnetization with the temperature. Below the critical temperature T_c, it is possible to observe a non-null magnetization. At minimum temperature ($T = 0$), the system will be in the most ordered phase, with magnetization at the saturation value. The antiferromagnetic case can also be described with a numerical approach. The result, naturally, will differ from the ferromagnetic case. Although there is order at low temperatures as spin covariance between sites is low, there will be no net magnetization at any temperature.

The Ising model only deals with one direction of spin interaction, usually modeled between z components of spin. Its natural generalization at a three-dimensional spin space is the Heisenberg model Hamiltonian, which accounts for interaction between the vector spins $\vec{S}_i$. A significant distinction between the Ising and the Heisenberg model resides in the models' symmetries. While Heisenberg has continuous symmetry, Ising only has discrete symmetry. This leads to Heisenberg's model having no spontaneous symmetry breaking for finite temperature in $d \leq 2$ dimensions, according to the Mermin-Wagner-Hohenberg theorem (MERMIN; WAGNER, 1966; HOHENBERG, 1967). However, for materials to be in the quantum regime, some specific environmental conditions must be satisfied. A fundamental condition for quantum phase transitions is that temperature must be set to zero ($T = 0$). This ensures systems will have no thermal fluctuations, and phase transitions will happen due to energy fluctuations of the ground state energy caused by variations of other parameters. Generally, the Hamiltonian will depend on a parameter g, having the generic form $H(g)$, and the system ground state will be a function of this parameter. Phase transitions continue to occur due to fluctuations, but

unlike the transitions depicted by the Ising model (which happens due to thermal fluctuation), the fluctuations will arise from Heisenberg's uncertainty principle.

Quantum phase transitions are observed in spin models formed by systems of fermions or bosons. They provide spin to the sites of magnetic materials. The disposition, structure, and spin value of sites affect the magnetic properties the material will display. An interesting class of materials is the ferrimagnetic ones.

1.2 FERRIMAGNETIC MATERIALS AND LADDER CHAINS

Ferrimagnetic materials (KONG et al., 2018) are formed by lattices whose spin sites have an antiferromagnetic coupling, but with different magnitudes of spin (SILVA, 2019). The lowest energy state would have all sites spin contrary aligned but, since the spins have different magnitudes, the magnetic material will display a spontaneous magnetization, as in the ferromagnetic case. These different magnitude spins can be due to unit cell structure, as well as magnetic ions with a different spin. When these systems are exposed to a magnetic field at zero temperature, they can go through quantum phase transitions. They involve transitions from gapped to gapless phases (RÜEGG et al., 2008), magnetic susceptibility divergences (WANG; YU, 2000), as well as the magnetization plateaus (LANGARI; MARTÍN-DELGADO, 2000), an important subject of this text.

Plateaus in the magnetization curves are not present in all types of materials. The open spin-$\frac{1}{2}$ chain, for instance, has no magnetization plateau in its magnetization curve, while the open spin-1 chain does, in accordance with Haldane's conjecture (AFFLECK, 1989). Magnetization plateaus can be observed in varied structures of ferrimagnetic mixed-spin chains, as observed in the multiple spin-($\frac{1}{2}$, S) chains (SILVA; MONTENEGRO-FILHO, 2021).

The mixed spin-1 and spin-$\frac{1}{2}$ ladder is composed of two coupled linear chains with mixed spins. There are two coupling variables that describe it: the coupling between chains J_1 and the coupling between spins throughout each linear chain J_0. The ferrimagnetic mixed spin-1 and spin-$\frac{1}{2}$ ladder is composed of positive couplings $J_0 > 0$ and $J_1 > 0$. It presents an energy degenerescence in the energy levels as a function of the total magnetization curve, in accordance with the Lieb-Mattis description of the energy levels. It also presents a magnetization plateau at magnetization $\frac{1}{3}$ of the saturation value, the $\frac{1}{3}$-plateau. The energy degenerescence at the energy levels curve corresponds to constant values of energy when magnetization ranges

at the interval between 0 and $\frac{1}{3}$ of the saturation value. These degenerate values of energy are the lowest energy values available. When submitted to a small magnetic field, magnetization immediately tends to the value of $\frac{1}{3}$, and the magnetization curve will present a plateau. With $J_1 < 0$, the $\frac{1}{3}$ plateau decreases its size, indicating a transition from a gapped to a gapless phase. Since this transition occurs at constant magnetization, it has no symmetry breaking, and it consists of a Kosterlitz-Thouless phase transition.

A system of spin-$\frac{1}{2}$ trimers, for example, may as well present a Kosterlitz-Thouless phase transition, depending on the system's Hamiltonian. Isotropic interacting spin-$\frac{1}{2}$ trimers (MONTENEGRO-FILHO; SILVA-JÚNIOR; COUTINHO-FILHO, 2022) will have the $\frac{1}{3}$-plateau in the magnetization curve (figure 1), but has no Kosterlitz-Thouless phase transition in its phase diagram (figure 2). Anisotropic interacting spin-$\frac{1}{2}$ trimers modeled with an anisotropic Heisenberg Hamiltonian (MONTENEGRO-FILHO; MATIAS; COUTINHO-FILHO, 2020), however, presents a Kosterlitz-Thouless phase transition in its phase diagram (figure 3).

Figura 1 – Magnetization per trimer as a function of the applied magnetic field for positive (a) and negative (b) spin coupling.

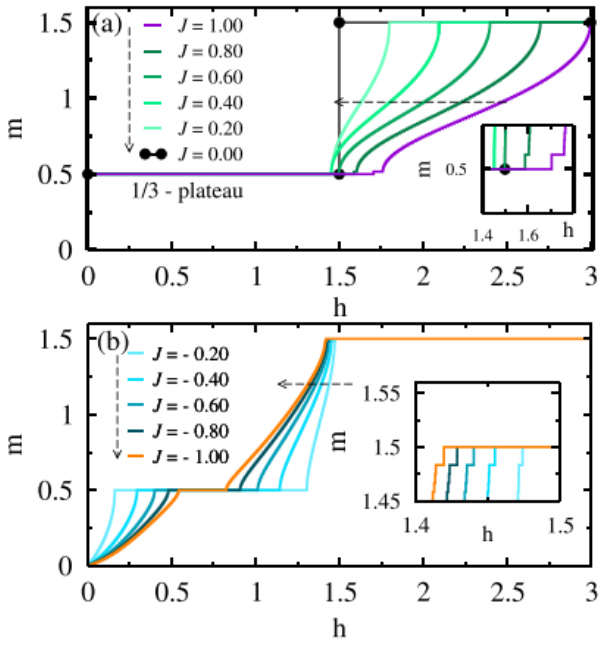

Source: (MONTENEGRO-FILHO; SILVA-JÚNIOR; COUTINHO-FILHO, 2022).

Figura 2 – a) Spin-$\frac{1}{2}$ trimers magnetic field (h) vs spin coupling ratio J phase diagram, with gapped phases ($\frac{1}{3}$-plateau) and gapless phases (Luttinger liquid). Note there is no Kosterlitz-Thouless phase transition, as the $\frac{1}{3}$-plateau does not close. b) Visual representation of the average spin orientation as a function of the spin coupling ratio J.

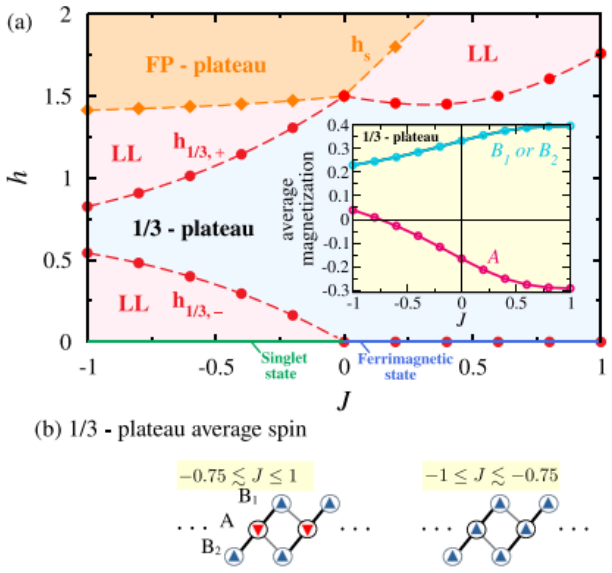

Source: (MONTENEGRO-FILHO; SILVA-JÚNIOR; COUTINHO-FILHO, 2022).

Figura 3 – a) Anisotropy of the Heisenberg Hamiltonian of the spin-$\frac{1}{2}$ trimer chain. b) Magnetization as a function of the applied magnetic field for different values of λ, the anisotropy parameter. c) Anisotropic spin-$\frac{1}{2}$ trimers magnetic field (h) vs anisotropy parameter (λ) phase diagram. There are gapped phases ($\frac{1}{3}$-plateau) and gapless phases (Luttinger liquid), as well as a Kosterlitz-Thouless phase transition.

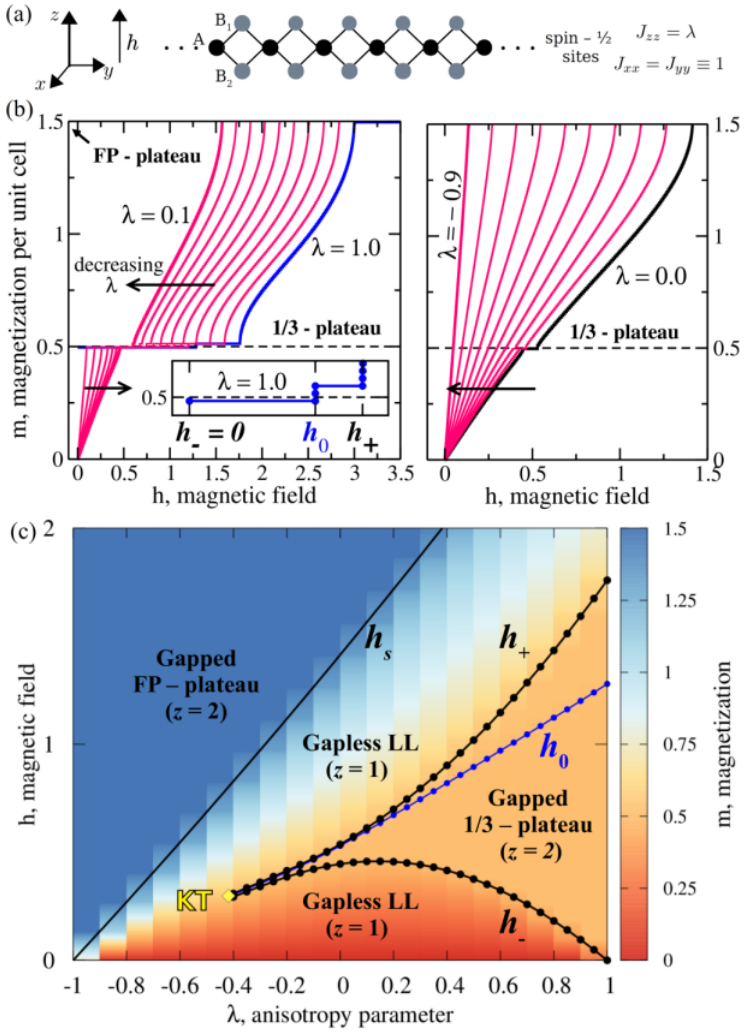

Source: (MONTENEGRO-FILHO; MATIAS; COUTINHO-FILHO, 2020).

Examples of ferrimagnetic lattice structures would be the open ferrimagnetic chain (figure 4) and the ferrimagnetic ladder (figure 5) with spin-1 and spin-$\frac{1}{2}$. The ladder structure is a recurrent and important structure family. There are many known compounds that have ladder structures. An example would be the vanadyl pyrophosphate $(VO)_2P_2O_7$ (JOHNSTON et al., 1987), while the cuprates $SrCu_2O_3$ (ISHIDA et al., 1994) and $Sr_2Cu_3O_5$ (AZUMA et al., 1994) have a two leg and three leg ladder structure, respectively (figure 6). Quasi-unidimensional compounds (COUTINHO-FILHO et al., 2008) with ferrimagnetic order can be highlighted. The bimetallic compound NiCu(pba)$(H_2O)_3$.$2H_2O$ (figure 7) has nickel atoms with spin $S_{Ni} = 1$, while copper atoms have spin $S_{Cu} = \frac{1}{2}$ is an example of ferrimagnetic compound. Another

example would be the $CuMn(S_2C_2O_2)\cdot 7.5H_2O$, as the copper atoms will have different spin than the manganese atom ($S_{Cu} \neq S_{Mn}$) (VERDAGUER et al., 1984).

Figura 4 – Ferrimagnetic chain with spin-1 and spin-$\frac{1}{2}$.

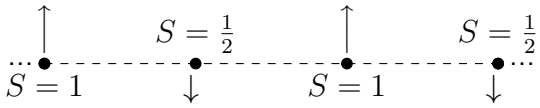

Source: the author (2022).

Figura 5 – Ferrimagnetic ladder with spin-1 and spin-$\frac{1}{2}$.

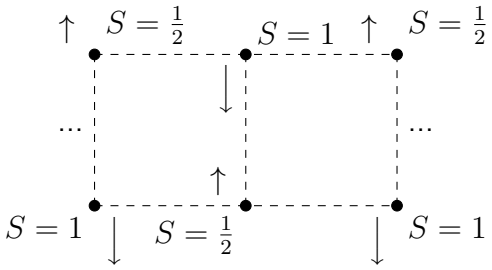

Source: the author (2022).

Figura 6 – Examples of compounds with ladder structure. a) $(VO)_2P_2O_7$ compound with ladder structure. b) $SrCu_2O_3$ compound with two-legged ladder structure. c) $Sr_2Cu_3O_5$ compound with three-legged ladder structure. J' and J are parameters of coupling between spins.

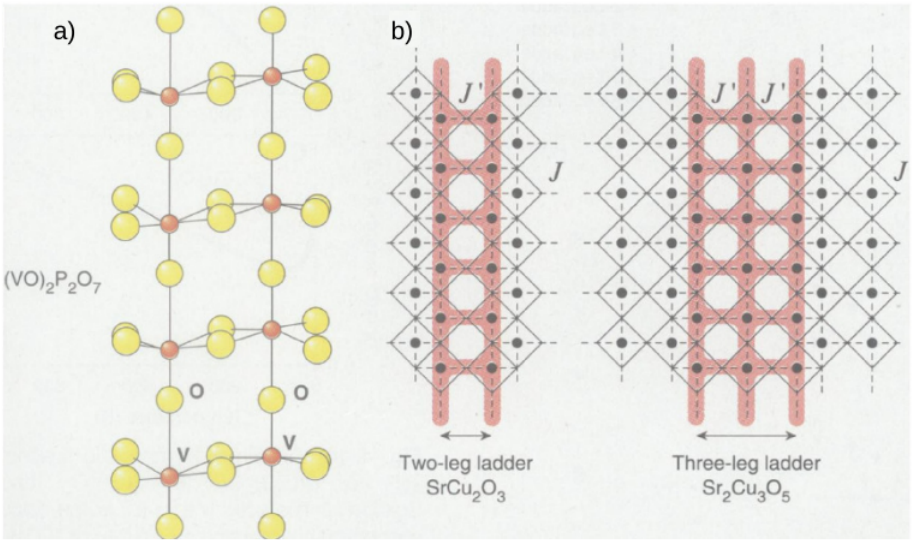

Source: (DAGOTTO; RICE, 1996).

Figura 7 – a) Bimetallic compound NiCu(pba)$(H_2O)_3$.$2H_2O$. b) Mixed-spin chain.

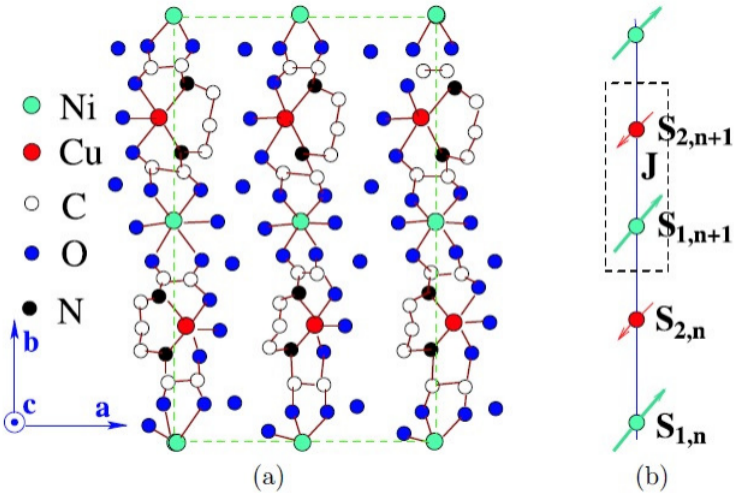

Source: (IVANOV, 2009).

1.3 DISSERTATION OUTLINE

This dissertation's main goal was to study quantum phase transitions of mixed spin-1 and spin-$\frac{1}{2}$ ladders. To accomplish this goal, multiple steps were taken.

The Hamiltonian of the Heisenberg model is defined in chapter 2, at first under no magnetic field, followed by a demonstration of its symmetry properties. The energy levels of the Heisenberg model under no magnetic field are shown to be eigenstates of the total spin S as well as the total spin in the z direction S^z, depicted by $E_0(S^z)$. Exact diagonalizations of the spin-$\frac{1}{2}$ and the mixed spin-1 and spin-$\frac{1}{2}$ Heisenberg dimers are obtained as an example. Later, it is discussed how an applied magnetic field introduces the Zeeman term into the Heisenberg model Hamiltonian, changing the energy levels of the Hamiltonian. It then concludes how magnetization curves are drawn using the energy levels $E_0(S^z)$ obtained at zero magnetic field.

The classification of phase transitions is elaborated in chapter 3 with the discussion of order parameters and correlation lengths. Then, there is a discussion of gapped and gapless systems, a fundamental concept for quantum phase transitions. The chapter is finalized with a description of quantum phase transitions, caused by a generic Hamiltonian parameter g.

Chapter 4 discusses the DMRG, an approximation method for solving the Heisenberg model Hamiltonian for one-dimensional systems. This method is fundamental to obtain the energy levels $E_0(S^z)$, used to obtain the magnetization curves since the Hilbert space dimension is

shown to grow exponentially with the chain size. The mathematical formulation of the density matrix and reduced density matrix are shown, and how these concepts apply to the DMRG method is elaborated. The steps of the DMRG iteration process are listed. At last, energy levels and magnetization curves of other spin-models are reproduced to show the DMRG is providing good results.

Chapter 5 shows the results of the DMRG for the mixed spin-1 and spin-$\frac{1}{2}$ ladder. This chapter is divided into three parts. At first, it discusses the energy levels and magnetization curve of a chain with purely antiferromagnetic coupling between sites (i.e. the chain has ferrimagnetic order) and shows the average magnetization orientation along the chain. It is shown that these chains will have a magnetization plateau. The second part shows these results (energy levels, magnetization curve, and average magnetization orientation) when the vertical coupling between sites is ferromagnetic while maintaining an antiferromagnetic coupling between horizontally neighboured sites. The magnetization plateau is seen to decrease as the vertical coupling between sites decreases below zero. An exponential dependence is obtained for the magnetization plateau size. A Kosterlitz-Thouless phase transition is observed, as the system transits from a gapped to a gapless phase by varying the spin coupling.

Chapter 6 summarizes the results obtained throughout the text and presents conclusions.

2 HEISENBERG MODEL HAMILTONIAN

The Hamiltonian is always a fundamental observable in the study of any physical system. It is through it that the system's available energies are calculated, as well as the time evolution of states and operators. This section will define the Hamiltonians used in the description of the magnetic materials in this text's scope.

2.1 HEISENBERG MODEL

The Hamiltonian of the Heisenberg model (MALVEZZI, 2003) for a magnetic insulator under no magnetic field is given by

$$H_0 = \sum_{i,j} J_{ij} \vec{S}_i \cdot \vec{S}_j, \tag{2.1}$$

where $\vec{S}_i$ is the spin vector at the site i. The term J_{ij} is such that $J_{ij} = J_{ji}$ and usually zero for sites that are not first neighbours, such that

$$H_0 = \sum_{<i,j>} J_{ij} \vec{S}_i \cdot \vec{S}_j, \tag{2.2}$$

where the notation $< i, j >$ represents that it must be counted only terms associated with the interaction of first neighbors. The interaction between two neighboring spins must be counted only once.

The calculation of eigenvalues of H_0 can be fairly complicated depending on the structure and size (number of unit cells L) of the magnetic material. The dimension of the Hilbert space is known to grow exponentially with the number of sites and exact diagonalization becomes a difficult task as L increases.

2.1.1 Dimension of Hilbert space and symmetries

For a single spin-$\frac{1}{2}$ site, a possible Hilbert space basis is the eigenstates of angular momentum in the z direction, given by

$$|\uparrow\rangle \, ; |\downarrow\rangle \text{ (Dimension: 2)},$$

so that the two sites with spin-$\frac{1}{2}$ basis can be written as

$$|\uparrow\uparrow\rangle\,;|\uparrow\downarrow\rangle\,;|\downarrow\uparrow\rangle\,;|\downarrow\downarrow\rangle \text{ (Dimension: 4)}.$$

The Hilbert space dimension can be generalized for a spin-$\frac{1}{2}$ chain with L unit cells: its dimension will be equal to $d = \underbrace{2 \times 2 ... \times 2}_{\text{L times}} = 2^L$. Naturally, as L increases, diagonalization becomes quite difficult to be performed, since d will diverge exponentially to infinity. Therefore, an approximation method is important to the subsequent evaluation of eigenstates of energy. However, there are symmetry properties that can simplify the determination of the Heisenberg model eigenstates. Those properties arise from commutation relations. The interest will lie in the two particular commutators

$$[H_0, S^z]\ ;\ [H_0, S^2],$$

with S^z as the total angular momentum in the z direction and S^2 is the total angular momentum, that is

$$S^2 = (S^x)^2 + (S^y)^2 + (S^z)^2;$$

$$S^l = \sum_i S_i^l, \text{ with } l = x, y, z.$$

In order to evaluate these commutators, the angular momentum commutation relations, valid for any angular momentum observable $\vec{S}$, will be used. They are given by

$$\vec{S} = S^x\hat{\mathbf{x}} + S^y\hat{\mathbf{y}} + S^z\hat{\mathbf{z}}; \tag{2.3}$$

$$[S^x, S^y] = i\hbar S^z; \tag{2.4}$$

$$[S^y, S^z] = i\hbar S^x; \tag{2.5}$$

$$[S^z, S^x] = i\hbar S^y. \tag{2.6}$$

The commutation $[H_0, S_k^z]$ between H_0 and the spin observable in z direction of a generic site k is equal to

$$[H_0, S_k^z] = \sum_{<i,j>} J_{ij}[\vec{S}_i \cdot \vec{S}_j, S_k^z].$$

The inner product term of interaction between spins i and j $\vec{S}_i \cdot \vec{S}_j$ is equal to

$$\vec{S}_i \cdot \vec{S}_j = S_i^x S_j^x + S_i^y S_j^y + S_i^z S_j^z.$$

The commutation relation $[\vec{S}_i \cdot \vec{S}_j, S_k^z]$ is then given by

$$[\vec{S}_i \cdot \vec{S}_j, S_k^z] = [S_i^x S_j^x, S_k^z] + [S_i^y S_j^y, S_k^z] + [S_i^z S_j^z, S_k^z].$$

The first term to be analyzed will be $[S_i^x S_j^x, S_k^z]$ and the analysis for $[S_i^y S_j^y, S_k^z]$ is analogous. $[S_i^z S_j^z, S_k^z]$ is always zero.

$$[S_i^x S_j^x, S_k^z] = -([S_k^z, S_i^x] S_j^x + S_i^x [S_k^z, S_j^x]);$$

$$[S_i^{\mathsf{x}} S_j^{\mathsf{x}}, S_k^{\mathsf{z}}] = -i\hbar(S_i^y S_j^x \delta_{ik} + S_i^x S_j^y \delta_{jk}). \tag{2.7}$$

For $[S_i^y S_j^y, S_k^z]$, it is valid that

$$[S_i^y S_j^y, S_k^z] = -([S_k^z, S_i^y] S_j^y + S_i^y [S_k^z, S_j^y]);$$

$$[S_i^y S_j^y, S_k^z] = i\hbar(S_i^x S_j^y \delta_{ik} + S_i^y S_j^x \delta_{jk}). \tag{2.8}$$

It follows that

$$[H_0, S_k^z] = i\hbar \sum_{<i,j>} J_{ij}(-S_i^y S_j^x \delta_{ik} - S_i^x S_j^y \delta_{jk} + S_i^x S_j^y \delta_{ik} + S_i^y S_j^x \delta_{jk}).$$

Given that

$$S^z = \sum_k S_k^z,$$

it follows that

$$[H_0, S^z] = i\hbar \sum_{<i,j>} J_{ij} \sum_k (-S_i^y S_j^x \delta_{ik} - S_i^x S_j^y \delta_{jk} + S_i^x S_j^y \delta_{ik} + S_i^y S_j^x \delta_{jk});$$

$$[H_0, S^z] = i\hbar \sum_{<i,j>} J_{ij}(-S_i^y S_j^x - S_i^x S_j^y + S_i^x S_j^y + S_i^y S_j^x) = 0.$$

Then

$$[H_0, S^z] = 0. \tag{2.9}$$

This leads to the conclusion that the Heisenberg Hamiltonian has rotation symmetry since angular momentum is the generator of rotations towards some axis. In this case, there will be rotation symmetry relative to the three-axis: x, y, and z. However, introducing a magnetic field, the remaining rotation symmetry axis will only be the one parallel to the magnetic field. Hence, in general, the magnetic field is described as being in the z direction. In order to obtain $[H_0, S^2]$, symmetry properties can be used. Equation (2.9) must remain valid if $z \to x$ or $z \to y$, therefore $[H_0, S^z] = [H_0, S^y] = [H_0, S^x] = 0$. Then

$$S^2 = (S^x)^2 + (S^y)^2 + (S^z)^2;$$

$$[H_0, S^2] = \underbrace{[H_0, (S^x)^2]}_{[H_0, S^x]S^x + S^x[H_0, S^x] = 0} + \underbrace{[H_0, (S^y)^2]}_{=0} + \underbrace{[H_0, (S^z)^2]}_{=0} = 0;$$

$$[H_0, S^2] = 0. \tag{2.10}$$

With these commutation relations demonstrated, it is possible to conclude that the eigenstates of H_0 are eigenstates of S^z (total angular momentum in direction z) and S^2 (total angular momentum) (MALVEZZI, 2003). So, for a lattice with any number of sites, there are two bases that should be highlighted:

Option A) Basis is given by the tensor product of the eigenstates of ${S_i}^2$ and ${S_i}^z$ of each individual site. This is the basis normally used.

Option B) Basis is given by eigenstates of S^2 (total angular momentum) and S^z (total angular momentum in z direction). This base can be written in terms of the previous basis using Clebsch-Gordon coefficients. These states are the eigenstates of H_0.

2.1.2 Heisenberg model, antiferromagnetism and ferromagnetism

The term $\langle \vec{S_i} \cdot \vec{S_j} \rangle$, with i and j corresponding to two first neighbors spins, is either positive or negative. If it is positive, there is an increase in energy, while if it is negative, there is a decrease in energy. On the other hand, for $J_{ij} \leq 0$, if it is positive, there will be a decrease in energy, while if it is positive, there will be an energy increase.

In accordance with the minimum energy principle, when $J_{ij} \geq 0$, the tendency will be of antiparallel alignment since this decreases energy. However, when $J_{ij} \leq 0$, the parallel orientation has lower energy, being the more probable state. It can be concluded that $J_{ij} \geq 0$

corresponds to an antiferromagnetic coupling while $J_{ij} \leq 0$ corresponds to a ferromagnetic coupling between the sites i and j.

2.1.3 Lieb-Mattis theorem

The Lieb-Mattis theorem (LIEB; MATTIS, 1962) describes an energy level ordering of the Heisenberg model Hamiltonian under no magnetic field for some specific spin couplings condition. The eigenstates of the Heisenberg model Hamiltonian are eigenstates of both total spin S and total spin in the z direction S^z. The values of S^z for a given value of S are given by $S^z = -S$, $-S+1$, ..., 0, ..., $S-1$, S and the level with total spin S has a degeneracy of $2S+1$. The values of S can have a multitude of ranges, with the minimum value most commonly found to be 0 and the maximum value of S will be represented here by the generic value S_{max}. The state $S^z = 0$ will have a representation in any S space, while the $S^z = 1$ state will have a representation in any $S > 0$ space, the $S^z = 2$ will have a representation in any $S > 1$ space and so on.

For lattices with sites that have different total spin, here represented by spin A and B (with values s_A^i and s_B^i), there is a total spin difference $\mathcal{S}$ given by

$$\mathcal{S} = |s_A - s_B|; \tag{2.11}$$

with

$$s_A = \sum_i s_A^i \tag{2.12}$$

and

$$s_B = \sum_i s_B^i. \tag{2.13}$$

The Lieb-Mattis theorem establishes conditions at which the total spin S state with the lowest energy available will correspond to the state with $S = \mathcal{S}$. Consider $E(S)$ the lowest energy value of a total S state. The theorem consists of two equations:

$$E(S) > E(\mathcal{S}), \text{ with } S < \mathcal{S}; \tag{2.14}$$

$$E(S+1) > E(S), \text{ with } S \geq \mathcal{S}. \tag{2.15}$$

2.1.4 Oshikawa-Yamanaka-Affleck conjecture

The importance of obtaining the energy levels at zero magnetic field is that they are fundamental to determining the curve magnetization as a function of a magnetic field. For curves with magnetization plateaus, it is valid that the magnetization at the plateau is quantized. The Oshikawa-Yamanaka-Affleck conjecture consists on the following: if the maximum spin of a unit cell is S and the magnetization per unit cell of the state with translation symmetry is m, the magnetization plateau exists only if $S - m = N$, with N an integer (OSHIKAWA; YAMANAKA; AFFLECK, 1997). However, the conjecture does not state that if $S-m = N$, with N an integer, there is a magnetization plateau.

2.2 MIXED SPIN LADDER COUPLING

The mixed spin ladder is formed by the repetition of the structure depicted in figure 8. The coupling J_{ij} between spins is depicted in figure 8 as well, indicating the interaction is different between vertically and horizontally neighboring spins.

Figura 8 – Unit cell of mixed spin ladder with sites spin-1 and spin-$\frac{1}{2}$ chain.

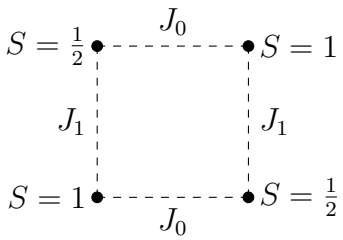

Source: the author (2022).

2.3 INTERACTION WITH AN APPLIED MAGNETIC FIELD

When an external magnetic field $\vec{B}$ is applied, the Hamiltonian of the system will be given by

$$H = \sum_{<i,j>} J_{ij}\vec{S_i} \cdot \vec{S_j} - h_B S^z. \tag{2.16}$$

Here, $h_B = \gamma B$, with γ the system's gyro magnetic factor. The Heisenberg Hamiltonian under magnetic field can then be written as

$$H = H_0 - h_B S^z. \tag{2.17}$$

Through commuting relations, it's possible to conclude that the eigenstates of H are the same of H_0, since

$$[H, S^z] = \underbrace{[H_0, S^z]}_{=0} - h_B \underbrace{[S^z, S^z]}_{=0} = 0;$$

$$[H, S^2] = \underbrace{[H_0, S^2]}_{=0} - h_B [S^z, S^2].$$

Breaking down the term $[S^z, S^2]$, it is valid that

$$[S^z, (S^x)^2] + [S^z, (S^y)^2] + [S^z, (S^z)^2] = [S^z, S^x]S^x + S^x[S^z, S^x] + [S^z, S^y]S^y + S^y[S^z, S^y] + 0;$$

$$[S^z, (S^x)^2] + [S^z, (S^y)^2] + [S^z, (S^z)^2] = i\hbar(S^y S^x + S^x S^y - SxS^y - S^y S^x) = 0;$$

$$[H, S^2] = [H, S^z] = 0. \tag{2.18}$$

Conclusion: the eigenstates of H_0 are eigenstates of H. However, the magnetic field provokes a shift in energy in states with $S^z \neq 0$. These shifts will be analyzed using the Heisenberg dimer as an example in the following section.

2.3.1 Heisenberg dimer

Consider two spin-$\frac{1}{2}$ sites with antiferromagnetic coupling (figure 9).

Figura 9 – Two spin-$\frac{1}{2}$ with antiferromagnetic coupling ($J > 0$) sites. Heisenberg dimer.

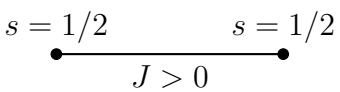

Source: the author (2022).

First, consider $h_B = 0$ and as a basis the eigenstates of S_1^z and S_2^z: $|\uparrow\uparrow\rangle$, $|\uparrow\downarrow\rangle$, $|\downarrow\uparrow\rangle$, $|\downarrow\downarrow\rangle$, which is used to write (2.2) in matrix form. For the lattice shown, H_0 will be given by

$$H_0 = J(S_1^x S_2^x + S_1^y S_2^y + S_1^z S_2^z).$$

Some useful identities are given by

$$S^x \left|\uparrow\right\rangle = \frac{\hbar}{2} \left|\downarrow\right\rangle, \; S^x \left|\downarrow\right\rangle = \frac{\hbar}{2} \left|\uparrow\right\rangle;$$

$$S^y \left|\uparrow\right\rangle = \frac{i\hbar}{2} \left|\downarrow\right\rangle, \; S^y \left|\downarrow\right\rangle = -\frac{i\hbar}{2} \left|\uparrow\right\rangle;$$

$$S^z \left|\uparrow\right\rangle = \frac{\hbar}{2} \left|\uparrow\right\rangle; \; S^z \left|\downarrow\right\rangle = -\frac{\hbar}{2} \left|\downarrow\right\rangle.$$

Applying H_0 to the basis' vectors, it is valid that

$$H_0 \left|\uparrow\uparrow\right\rangle = J \left(\frac{\hbar}{2}\right)^2 (\left|\uparrow\uparrow\right\rangle);$$

$$H_0 \left|\uparrow\downarrow\right\rangle = J \left(\frac{\hbar}{2}\right)^2 (2 \left|\downarrow\uparrow\right\rangle - \left|\uparrow\downarrow\right\rangle);$$

$$H_0 \left|\downarrow\uparrow\right\rangle = J \left(\frac{\hbar}{2}\right)^2 (2 \left|\uparrow\downarrow\right\rangle - \left|\downarrow\uparrow\right\rangle);$$

$$H_0 \left|\downarrow\downarrow\right\rangle = J \left(\frac{\hbar}{2}\right)^2 (\left|\downarrow\downarrow\right\rangle).$$

H_0 in matrix form is equal to

$$H_0 = J \left(\frac{\hbar}{2}\right)^2 \begin{bmatrix} 1 & 0 & 0 & 0 \\ 0 & -1 & 2 & 0 \\ 0 & 2 & -1 & 0 \\ 0 & 0 & 0 & 1 \end{bmatrix}.$$

Proceeding with diagonalization of H_0, it is valid that

$$\det \begin{bmatrix} 1-\lambda & 0 & 0 & 0 \\ 0 & -1-\lambda & 2 & 0 \\ 0 & 2 & -1-\lambda & 0 \\ 0 & 0 & 0 & 1-\lambda \end{bmatrix} = 0.$$

The characteristic polynomial is then given by

$$(1-\lambda)[(-1-\lambda)^2(1-\lambda)-4(1-\lambda)]=0.$$

Values for λ: $\lambda=1$ and $\lambda=-3$.

Eigenvalues of energy: $E_0=J(\frac{\hbar}{2})^2$ and $E_0=-3J(\frac{\hbar}{2})^2$.

The eigenstates and the energies are given by

$$\lambda=1, E_0=J\left(\frac{\hbar}{2}\right)^2 \text{ (Triplet states) } \begin{cases} |\uparrow\uparrow\rangle \\ \frac{|\uparrow\downarrow\rangle+|\downarrow\uparrow\rangle}{\sqrt{2}} \\ |\downarrow\downarrow\rangle \end{cases}$$

$$\lambda=-3, E_0=-3J\left(\frac{\hbar}{2}\right)^2 \text{ (Singlet state) } \begin{cases} \frac{|\uparrow\downarrow\rangle-|\downarrow\uparrow\rangle}{\sqrt{2}} \end{cases}$$

The eigenstates could be written in the base of total S^2 and total S^z as

$$\lambda=1, E_0=J\left(\frac{\hbar}{2}\right)^2 \text{ (Triplet states) } \begin{cases} |s=1,m=1\rangle \\ |s=1,m=0\rangle \\ |s=1,m=-1\rangle \end{cases}$$

$$\lambda=-3, E_0=-3J\left(\frac{\hbar}{2}\right)^2 \text{ (Singlet state) } \begin{cases} |s=0,m=0\rangle \end{cases}$$

Now, consider $h_B\neq 0$. The Hamiltonian will correspond to equation (2.17), and states with $S^z\neq 0$ will have a shift in its energy level.

The energy levels will be shifted in the following form

$$E(m)=E_0(m)-\underbrace{h_B m\hbar}_{\text{Energy shift}}. \tag{2.19}$$

$E_0(m)$ is the energy level when $h_B=0$ and m the eigenvalue associated with S^z.

For the triplet states ($\lambda=1$, $E_0=J(\frac{\hbar}{2})^2$), it is valid that

$|s=1,m=1\rangle$. This state has an energy shift when $h_B\neq 0$, since $m=1$, so $E(m)=J(\frac{\hbar}{2})^2-h_B\hbar$.

$|s=1,m=0\rangle$. This state does not have an energy shift when $h_B\neq 0$, since $m=0$, so $E(m)=J(\frac{\hbar}{2})^2$.

$|s = 1, m = -1\rangle$. This state has an energy shift when $h_B \neq 0$, since $m = -1$, so $E(m) = J(\frac{\hbar}{2})^2 + h_B\hbar$.

For the singlet state ($\lambda = -3$, $E_0 = -3J(\frac{\hbar}{2})^2$), it is valid that

$|s = 0, m = 0\rangle$. This state does not have an energy shift when $h_B \neq 0$, since $m = 0$, so $E(m) = -3J(\frac{\hbar}{2})^2$.

The energy levels $E(m)$ become functions of h_B (figure 10).

Figura 10 – $E(m)$ as a function of h_B for the triplet and singlet states.

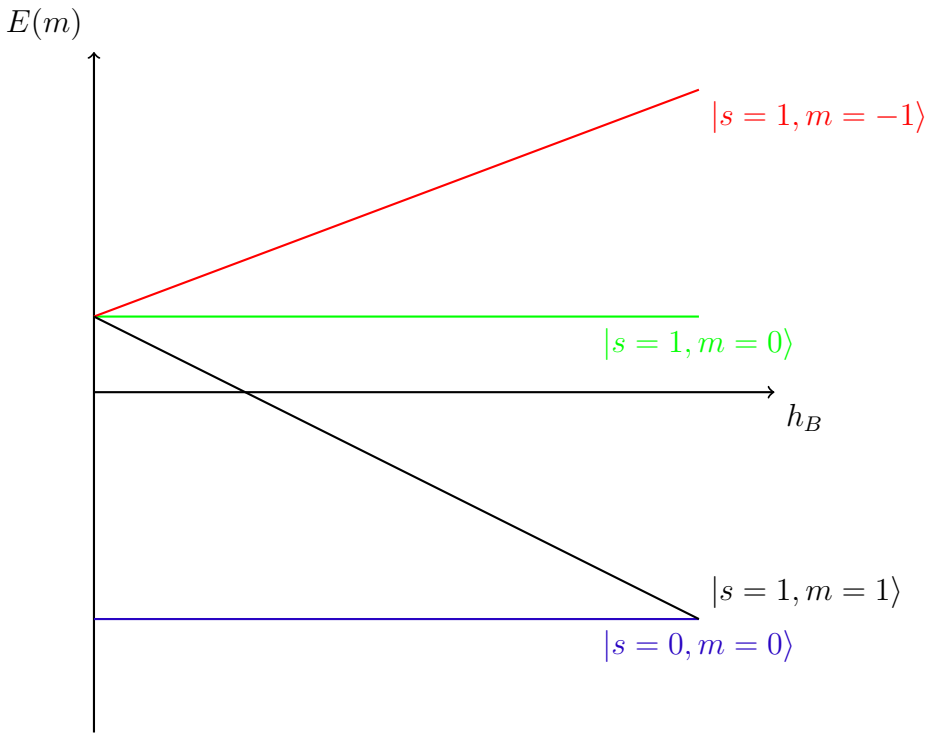

Source: the author (2022).

There is a value of h_B in which the energies of the triplet state $|s = 1, m = 1\rangle$ and singlet state $|s = 0, m = 0\rangle$ become the same. This transition describes an increase in the magnetization (GIAMARCHI; RÜEGG; TCHERNYSHYOV, 2008). An increase in h_B provoked a leap in the magnetization from $m = 0$ to $m = 1$, an increase of $\Delta m = 1$. In terms of S^z, there was an increase of $\Delta S^z = \hbar$.

Classically, magnetic dipole tends to align with the magnetic field. With a magnetic field increase, the magnetization grows in the direction of the field up to a saturation value, where the magnetization curve reaches a plateau.

The antiferromagnetic spin-$\frac{1}{2}$ Heisenberg dimer is a good representation for some magnetic insulators such as the $KCuCl_3$ and the $TiCuCl_3$ (RÜEGG et al., 2003). The ground state corres-

ponds to magnetization zero per dimer at zero magnetic field, the state of the insulator at zero temperature. As the magnetic field increases, the energy level with magnetization saturated will decrease due to the Zeeman term, leading to a magnetization increase once this energy level becomes the new ground state.

2.3.2 Heisenberg dimer with mixed spin-1 and spin-$\frac{1}{2}$

Consider now a Heisenberg dimer with mixed spin-1 and spin-$\frac{1}{2}$ with antiferromagnetic coupling (figure 11) under no magnetic field ($h_B = 0$).

Figura 11 – Spin-1 and spin-$\frac{1}{2}$ with ferromagnetic coupling ($J > 0$).

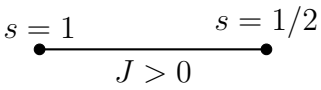

Source: the author (2022).

The Hilbert space dimension automatically increases from 4 for the case of two spin-$\frac{1}{2}$ sites to 6 for the spin-1 and spin-$\frac{1}{2}$ sites. The matrix for H_0 will become a 6 by 6 (opposed to the 4 by 4 in the previous case). The eigenstates are known to be the basis vectors of the total angular momentum operators S^2 and S^z. This information will be used in this section to show a different approach to diagonalizing H_0.

Consider that each site is labeled by 1 and 2, with 1 referring the site with spin-1, while 2 references the site with spin-$\frac{1}{2}$. Then, the basis for the spin at each site will be represented by a generic ket of the form $|m_1, m_2\rangle$, with

$$S_1^z |m_1, m_2\rangle = m_1 \hbar |m_1, m_2\rangle ;$$

$$S_2^z |m_1, m_2\rangle = m_2 \hbar |m_1, m_2\rangle ;$$

$$S_1^2 |m_1, m_2\rangle = 2\hbar^2 |m_1, m_2\rangle ;$$

$$S_2^2 |m_1, m_2\rangle = \frac{3}{4}\hbar^2 |m_1, m_2\rangle .$$

The values of m_1 and m_2 are given by $m_1 = -1,\ 0,\ 1$ and $m_2 = -\frac{1}{2},\ \frac{1}{2}$. The total m associated with the total S^z will then have values of $m = -\frac{3}{2},\ -\frac{1}{2},\ \frac{1}{2},\ \frac{3}{2}$. The eigenstates of H_0 will be represented in the same way as before: $|s, m\rangle$.

Starting with the state $|s = 3/2, m = 3/2\rangle = |1, 1/2\rangle$ the other states are obtained using the J_+ and J_- angular momentum operators, in the same way through which the Clebsch-Gordon coefficients are obtained, that is

$$J_+ = J_x + iJ_y;$$

$$J_- = J_x - iJ_y.$$

When applied to a generic $|j, m\rangle$, they operate as the relations

$$J_+ |j, m\rangle = \hbar\sqrt{j(j+1) - m(m+1)}\, |j, m+1\rangle \tag{2.20}$$

$$J_- |j, m\rangle = \hbar\sqrt{j(j+1) - m(m-1)}\, |j, m-1\rangle \tag{2.21}$$

The state $|1, 1/2\rangle$ must correspond to the state $|s = 3/2, m = 3/2\rangle$, since $|1, 1/2\rangle$ has the highest value of $m = m_1 + m_2 = \frac{3}{2}$. From $|1, 1/2\rangle = |s = 3/2, m = 3/2\rangle$ and

$$S_- = S_{1-} + S_{2-};$$

it is possible to find

$$S_- |s = 3/2, m = 3/2\rangle = \hbar\sqrt{3}\, |s = 3/2, m = 1/2\rangle\,;$$

$$S_- |s = 3/2, m = 3/2\rangle = \hbar(\sqrt{2}\, |0, 1/2\rangle + |1, -1/2\rangle\,;$$

Then,

$$|s = 3/2, m = 1/2\rangle = \sqrt{\frac{2}{3}}\, |0, 1/2\rangle + \sqrt{\frac{1}{3}}\, |1, -1/2\rangle\,.$$

The state $|s = 1/2, m = 1/2\rangle$ must be a linear combination of the states $|0, 1/2\rangle$ and $|1, -1/2\rangle$, so that

$$|s = 1/2, m = 1/2\rangle = a\, |0, 1/2\rangle + b\, |1, -1/2\rangle\,.$$

Also, $|s = 1/2, m = 1/2\rangle$ must be orthonormal to $|s = 3/2, m = 1/2\rangle$. A possible solution for a and b is given by $a = \sqrt{\frac{1}{3}}$ and $b = -\sqrt{\frac{2}{3}}$, which leads to

$$|s = 1/2, m = 1/2\rangle = \sqrt{\frac{1}{3}}\,|0, 1/2\rangle - \sqrt{\frac{2}{3}}\,|1, -1/2\rangle\,.$$

Both states $|s = 3/2, m = 1/2\rangle$ and $|s = 1/2, m = 1/2\rangle$ have the same total S^z, but the interest will lie in the state with the least energy, since this state will have a level crossing sooner, as in figure 10. It is unnecessary to analyze the states with negative S^z value since the Hamiltonian is invariant under the transformation $S_i^z \rightarrow -S_i^z$ for all i. In general, magnetization curves can be plotted using only the energy levels with positive total S^z: the negative S^z region will have the same results due to symmetry. The states found are listed below.

$$|s = 3/2, m = 1/2\rangle = \sqrt{\frac{2}{3}}\,|0, 1/2\rangle + \sqrt{\frac{1}{3}}\,|1, -1/2\rangle\,;$$

$$|s = 1/2, m = 1/2\rangle = \sqrt{\frac{1}{3}}\,|0, 1/2\rangle - \sqrt{\frac{2}{3}}\,|1, -1/2\rangle\,;$$

$$|s = 3/2, m = 3/2\rangle = |1, 1/2\rangle\,.$$

It is convenient to write the Hamiltonian H_0 as

$$H_0 = J\left[\frac{1}{2}(S_{1+}S_{2-} + S_{1-}S_{2+}) + S_{1z}S_{2z}\right]; \tag{2.22}$$

Applying H_0 to these states, it is expected to find $H_0\,|s, m\rangle = E_0\,|s, m\rangle$ and one can verify that

$$H_0\,|s = 3/2, m = 1/2\rangle = \frac{J\hbar^2}{2}\,|s = 3/2, m = 1/2\rangle\,;$$

$$H_0\,|s = 1/2, m = 1/2\rangle = -J\hbar^2\,|s = 1/2, m = 1/2\rangle\,;$$

$$H_0\,|s = 3/2, m = 3/2\rangle = \frac{J\hbar^2}{2}\,|s = 3/2, m = 3/2\rangle\,;$$

The energy levels $E_0(S^z)$ as functions of total S^z are then given by

$$E_0(3\hbar/2) = \frac{J\hbar^2}{2};$$

$$E_0(\hbar/2) = -J\hbar^2.$$

The energy level of the state $|s = 3/2, m = 1/2\rangle$ is the same energy of the state $|s = 3/2, m = 3/2\rangle$, meaning there is a degeneracy. A magnetic field in the z direction will break this invariance. The energy levels that will interest will always be the lowest value available for each total S^z since they will cross first with the previous S^z level as the magnetic field increases. At zero magnetic field, the system state will be $|s = 1/2, m = 1/2\rangle$. As the magnetic field increases, the state $|s = 3/2, m = 3/2\rangle$ energy will decrease and, eventually, become lower than the $|s = 1/2, m = 1/2\rangle$, and magnetization will increase from the $m = 1/2$ to $m = 3/2$.

2.4 MAGNETIZATION CURVE

Since the Heisenberg model Hamiltonian's energy levels are eigenstates of the total S^z, the lowest energy values for each S^z at zero magnetic field ($h_B = 0$) will be depicted as $E_0(S^z)$. Naturally, the total S^z relates to the eigenvalue m through the relation $S^z = m\hbar$. When $h_B = 0$, antiferromagnetic materials display energy levels $E_0(S^z)$ that are more energetic the greater the value of total S^z. However, when the magnetic field is turned on ($h_B > 0$), the levels with higher S^z will have higher decreases in energy. Since the lowest value of total S^z is zero (which corresponds to $m = 0$), in general, this tends to be the lowest energy level of antiferromagnetic materials when $h_B = 0$, depicted by $E_0(m = 0) = E_0(0)$. The level $m = 1$ has higher energy than the $m = 0$ level, but its energy decreases as h_B increases. Eventually, the levels $m = 0$ and $m = 1$ will cross at some value of h_B, and the level $m = 1$ becomes the new ground state. If h_B keeps increasing, the energy level of $m = 2$ will decrease even further than the level $m = 1$, and the level $m = 2$ will become the new lowest energy state, at which the m eigenvalue will increase by one. Consider the lowest energy values $E_0(m)$ for each possible m of the Heisenberg Hamiltonian with $h_B = 0$. According to equation (2.19), the levels $E(m + 1)$ and level $E(m)$ will be given by

$$E(m + 1) = E_0(m + 1) - h_B(m + 1)\hbar;$$

$$E(m) = E_0(m) - h_B m\hbar.$$

The level crossing occurs when h_B is such that the two energy levels match, that is

$$E(m+1) = E_0(m+1) - h_B(m+1)\hbar = E(m) = E_0(m) - h_B m\hbar;$$

$$E_0(m+1) - E_0(m) = h_B\hbar;$$

$$h_B = \frac{E_0(m+1) - E_0(m)}{\hbar}. \tag{2.23}$$

This is the value of h_B for which the levels m and $m+1$ have the same energy and the eigenvalue m difference is $\Delta m = 1$. The investigation towards magnetization increase is achieved through the determination of the energy levels $E_0(m)$, so exact diagonalization of H_0 must be achieved. As was discussed in section 2.1.1, exact diagonalization becomes increasingly hard as the system size increases. Therefore, it is necessary to use computational algorithms to diagonalize H_0. While implementing a computational algorithm, it is common to set $\hbar = 1$. The crossing of energy levels is described by the equations

$$\Delta S^z = 1 \text{ (Increase from } S^z \text{ to } S^z + 1); \tag{2.24}$$

$$h_B = E_0(m+1) - E_0(m) = E_0(S^z + 1) - E_0(S^z). \tag{2.25}$$

Once these equations are set, it can now be answered what magnetic field it is expected that magnetization will grow for both cases of Heisenberg dimer discussed at 2.3.1 and 2.3.2. For the Heisenberg dimer with spin-$\frac{1}{2}$, it is valid that

$$|s = 0, m = 0\rangle\,, \text{ with energy } E_0 = -\frac{3J}{4};$$

$$|s = 1, m = 1\rangle\,, \text{ with energy } E_0 = \frac{J}{4}.$$

The magnetic field that increases magnetization from state $|s = 0, m = 0\rangle$ to state $|s = 1, m = 1\rangle$ is then given by

$$h_B = J.$$

For the mixed spin-1 and spin-$\frac{1}{2}$ Heisenberg dimer, the levels are given by

$$|s = 1/2, m = 1/2\rangle\,, \text{ with energy } E_0 = -J;$$

$$|s = 3/2, m = 3/2\rangle\,, \text{ with energy } E_0 = \frac{J}{2}.$$

To increase magnetization from state $|s = 1/2, m = 1/2\rangle$ to state $|s = 3/2, m = 3/2\rangle$, the applied magnetic field must be

$$h_B = \frac{3J}{2}.$$

The magnetization curves are obtained using the energy levels of the Heisenberg Hamiltonian at zero magnetic field $E_0(S^z)$. The plot usually takes a step form for finite systems, since the value h_B^+ (or h_B^-) is the value at which the levels $S^z + 1$ and S^z have the same energy (or S^z and $S^z - 1$ match). This means that, at these values of a magnetic field, the system can be at either state of magnetization. For the h_B^+ curve, at slightly higher values of a magnetic field, the magnetization leaps to $S^z + 1$, while at slightly smaller values of a magnetic field the magnetization stays at S^z. The discussion is similar to the h_B^- curve. In order to obtain the magnetization curve's points, there are two point-generating equations. They are

$$h_B^+ = E_0(S^z + 1) - E_0(S^z), \text{ point } (h_B^+,\, S^z); \tag{2.26}$$

$$h_B^- = E_0(S^z) - E_0(S^z - 1), \text{ point } (h_B^-,\, S^z). \tag{2.27}$$

2.4.1 Magnetization plateau and second order phase transition

In the thermodynamic limit, an increase of 1 at the total S^z corresponds to a small increase compared to the saturation value: an infinitesimal increase. It is expected that the magnetization increases little when leaping from a total S^z level to the level $S^z + 1$, and the step form of the magnetization curve as a function of the applied magnetic field will become unnoticeable. The value of magnetic field h_B that increases the system magnetization is the one that makes the energy levels of the total S^z state have the same energy as the level $S^z + 1$. At this value of a magnetic field, the partial derivative of the total S^z energy level under an applied magnetic field $E(S^z)$ with respect to the total S^z will be zero, that is

$$\left.\frac{\partial E}{\partial S^z}\right|_{h_B} = 0.$$

Demonstration of this relation is straightforward: since $E(S^z) = E(S^z + \Delta S^z)$ at this value of magnetic field h_B, it follows that

$$[E(S^z + \Delta S^z) - E(S^z)]\Big|_{h_B} = 0,$$

then

$$\frac{\partial E}{\partial S^z}\Big|_{h_B} = \frac{E(S^z + \Delta S^z) - E(S^z)}{\Delta S^z}\Big|_{h_B} = 0.$$

The energy level of the state with total S^z is equal to

$$E(S^z) = E_0(S^z) - h_B S^z, \tag{2.28}$$

with $E_0(S^z)$ the lowest energy state with total S^z under no magnetic field, the transition field h_B is the one at which, in the thermodynamic limit, it is valid that

$$\frac{\partial E}{\partial S^z}\Big|_{h_B} = 0. \tag{2.29}$$

Replacing (2.28) at (2.29) will result in

$$\frac{\partial E}{\partial S^z} = \frac{\partial E_0}{\partial S^z} - h_B = 0;$$

$$h_B = \frac{\partial E_0}{\partial S^z}. \tag{2.30}$$

Hence, the slope of the energy levels $E_0(S^z)$ at zero magnetic field curve will provide the magnetic field at each total S^z value, making possible the plot of the magnetization as a function of the magnetic field.

Some energy curves will lead to magnetization plateaus in the thermodynamic limit, where magnetization remains constant at a finite interval of h_B. Magnetization plateaus occur due to sharp points at the energy curve, since the derivative in equation (2.30) will have a discontinuity. Magnetic susceptibility χ is another important variable of magnetic systems. It is defined as the total magnetization response to an applied magnetic field, given by

$$\chi = \frac{\partial S^z}{\partial h_B}. \tag{2.31}$$

It is connected to the second partial derivative of the energy levels E_0 through the cyclic chain rule

$$\chi = \left(\frac{\partial h_B}{\partial S^z}\right)^{-1}. \tag{2.32}$$

Equation (2.32) is connected to the second partial derivative of the energy levels E_0, that is

$$\frac{\partial h_B}{\partial S^z} = \frac{\partial^2 E_0}{\partial {S^z}^2}. \tag{2.33}$$

The partial derivative of (2.33) will be connected to the difference between the fields h_B^+ and h_B^- defined at equations (2.26) and (2.27) and it is given by

$$h_B^+ - h_B^- = E_0(S^z + 1) - 2E_0(S^z) + E_0(S^z - 1).$$

This difference will depend on the structure of the magnetic chain. Some chains' magnetization curves will lead to divergences in the magnetic susceptibility at critical points. This is the case of the mixed spin-1 and spin-$\frac{1}{2}$ ladder, which will be presented later. At magnetization plateaus, total S^z remains constant at a h_B interval, meaning that

$$\frac{\partial S^z}{\partial h_B} = 0,$$

and susceptibility χ will be null. If the difference $h_B^+ - h_B^-$ tends to zero, the partial derivative $\frac{\partial h_B}{\partial S^z}$ will tend to zero as well, that is

$$\frac{\partial h_B}{\partial S^z} \to 0.$$

In this case, the susceptibility will diverge according to equation (2.32), configuring a second-order phase transition.

3 PHASE TRANSITIONS

This section will elaborate on fundamental concepts of phase transitions (such as order parameters and correlation length), describe first- and second-order phase transitions, discuss the topological phase transition of Kosterlitz-Thouless, elaborate the concept of gapped and gapless systems and quantum phase transitions.

3.1 ORDER PARAMETER, CORRELATION LENGTH, AND CLASSIFICATION OF PHASE TRANSITIONS

Phase transitions can be mathematically described by a variable known as order parameter Θ. It usually is non-null when the applied field (temperature, pressure, magnetic field, etc) is below a critical value, and null when the applied field is greater than the critical value. As an example, the Ising model describes a phase transition for ferromagnetic materials, as magnetization is non-null below a critical limit T_c and null for $T > T_c$. The appropriate order parameter Θ here would be the net magnetization. Another example would be the water thermal phase transitions. At atmospheric pressure, water can exist as a solid when the temperature is below 273K and as a liquid for temperatures above 273K. The critical temperature then is given by $T_c = 273K$ and it is convenient to define the order parameter by $\Theta = \rho - \rho_l$, with ρ_l the density at liquid phase and ρ the density at any phase. For $T < T_c$, it is valid that $\Theta \neq 0$ and, for $T > T_c$, $\Theta = 0$ (assuming that T is below $373K$), configuring a phase transition.

The correlation length ξ is another variable that provides essential information about phase transitions. It measures the range of correlation of any physical system. Consider a ferromagnetic chain described by the Ising model for example. For temperatures above T_c, the system is not organized and spin orientation will be random, with no long-range order, and the correlation length will be zero. Decreasing the temperature towards T_c, the order is increased as the spins will tend to have the same orientation. The correlation length increases continuously as the temperature approaches T_c from above. Below T_c, there will be long-range order, and the correlation length is expected to diverge to infinity. In this case, the correlation length is given by a power law, with $\xi \propto (T - T_c)^{-\gamma}$ and α a positive constant.

There is a difference between the described water phase transition and the ones described

by the Ising model. Water has an abrupt change in its density. Ferromagnetic materials, on the other hand, will have a continuous (yet fast) decreasing magnetization with the temperature. This distinction leads to a different classification for each type of phase transition. In Ehrenfest classification, first-order phase transitions would exhibit discontinuities in the first derivative of the free energy with respect to some thermodynamic variable. In this sense, the second-order phase transition would exhibit a discontinuity in the second derivative of the free energy. There could be higher-order phase transitions, depending on the discontinuities of the higher-order derivatives of free energy. The modern classification of phase transitions differs slightly from Ehrenfest's classification. First-order phase transitions are transitions that require receiving or releasing a typically large amount of energy to happen. In transitions like these, order parameters would not have a continuous form, as the water ice-liquid phase transition described previously. Second-order phase transitions are continuous phase transitions, in which the correlation length is a continuous function with a power law dependence.

Another phase transition form is the quantum phase transition. They are transitions between different quantum states provoked by an applied field at zero temperature.

The Kosterlitz-Thouless phase transition (KOSTERLITZ; THOULESS, 1973; KOSTERLITZ, 1974) is a topological phase transition (CONTINENTINO, 2017). It is continuous, but with no symmetry breaking. Some spin-interacting systems display this transition, such as the ones studied in (MONTENEGRO-FILHO; MATIAS; COUTINHO-FILHO, 2020). The correlation length will have an exponential form dependency in this transition (ZHENG; SCHULZ; TRIMPER, 1999), instead of a power law as in a second-order phase transition.

3.2 GAPPED AND GAPLESS HAMILTONIAN

The systems of interest while studying phase transitions are ones composed of many particles. The many-particles condition is referenced as the thermodynamic limit, when the number of particles would tend to infinity. In order for a Hamiltonian to be denominated gapped, there must be a finite energy difference between the system's ground state and the first excited state when the energy levels are evaluated in the thermodynamic limit. Else, it is gapless.

Infinity, however, is an abstract concept. The numeric process can not portray precisely an idea of infinity. A possibility to investigate gapped or gapless phases is to evaluate the energy levels for multiple system sizes L_i. For distinct L_i values, the energy levels will be different.

Consider E_0 the ground state and E_1 the first excited state. The energy gap is then given by $\Delta = E_1 - E_0$. Should Δ converge to a finite value as L_i increases, the Hamiltonian is gapped. Else, the Hamiltonian is gapless. This is a piece of important information since the investigation of thermodynamic limit for spin interacting systems can be achieved by performing finite-size scale analysis.

3.3 QUANTUM PHASE TRANSITIONS

Quantum phase transitions occur at zero temperature and are caused by a Hamiltonian parameter. The parameter that induces transitions will be denoted by g and its value changes the system's ground state, leading up to quantum phase transitions (SACHDEV, 2011; SACHDEV; KEIMER, 2011). Let a system's Hamiltonian H have an arbitrary dependence on a parameter g such that $H = H(g)$ and the temperature T be set to zero. Its energy eigenvalues $E(g)$ will also be a function of the parameter g. The system will necessarily be on the ground state. Since the eigenvalues of energy are functions of g, this parameter can transit the system to different quantum states.

As a way to illustrate the system's state dependency on the value of g, consider $H(g) = H_0 + gH_1$, with $[H_0, H_1] = 0$. The eigenstates of $H(g)$ are simultaneously eigenstates of H_0 and H_1. Then, for an eigenstate of H_0 and H_1 $|a_0, a_1\rangle$ with

$$H_0 |a_0, a_1\rangle = a_0 |a_0, a_1\rangle ;$$

$$H_1 |a_0, a_1\rangle = a_1 |a_0, a_1\rangle ;$$

$$a_0 > 0;$$

$$a_1 > 0.$$

It is valid that $H(g) |a_0, a1\rangle = (a_0 + ga_1) |a_0, a_1\rangle$ and this state's energy $E(g)$ will be equal to

$$E_a(g) = a_0 + ga_1.$$

Suppose another eigenstate of H_0 and H_1 $|b_0, b_1\rangle$ with

$$H_0 |b_0, b_1\rangle = b_0 |b_0, b_1\rangle ;$$

$$H_1 |b_0, b_1\rangle = b_1 |b_0, b_1\rangle ;$$

$$b_0 > a_0;$$

$$b_1 < 0.$$

This state's energy will be equal to

$$E_b(g) = b_0 + gb_1.$$

It will be assumed that a_0 is the ground state energy of H_0, while b_0 is the first excited state energy. When $g = 0$, the state $|a_0, a_1\rangle$ is the ground state, which will be the system's state. As g grows, with $a_1 > 0$ and $b_1 < 0$, it comes clear that the energy levels must cross at some point $g = g_c$ (figure 12). When $g > g_c$, there is an inversion: the state $|b_0, b_1\rangle$ becomes the new ground state and the system will transit to this new ground state.

Figura 12 – Energy levels for the states $|a_0, a_1\rangle$ and $|b_0, b_1\rangle$.

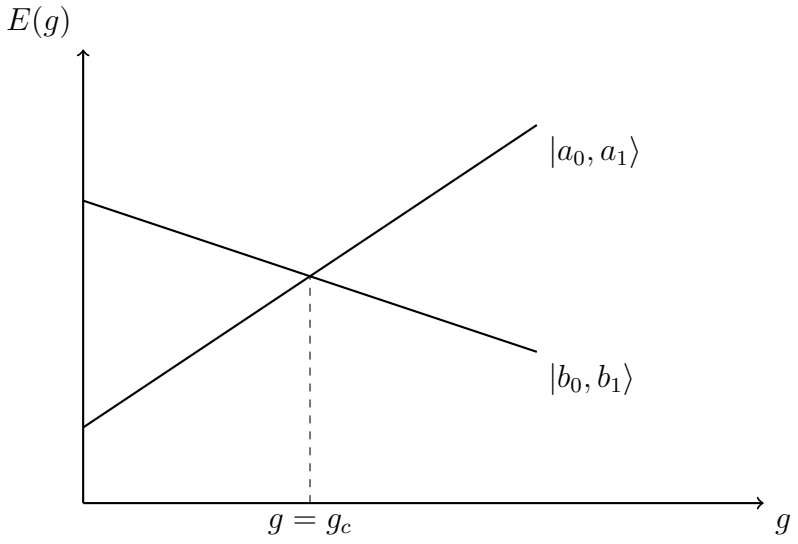

Source: the author (2022).

Figura 13 – Lowest energy states of $H(g)$ displaying an avoided level crossing.

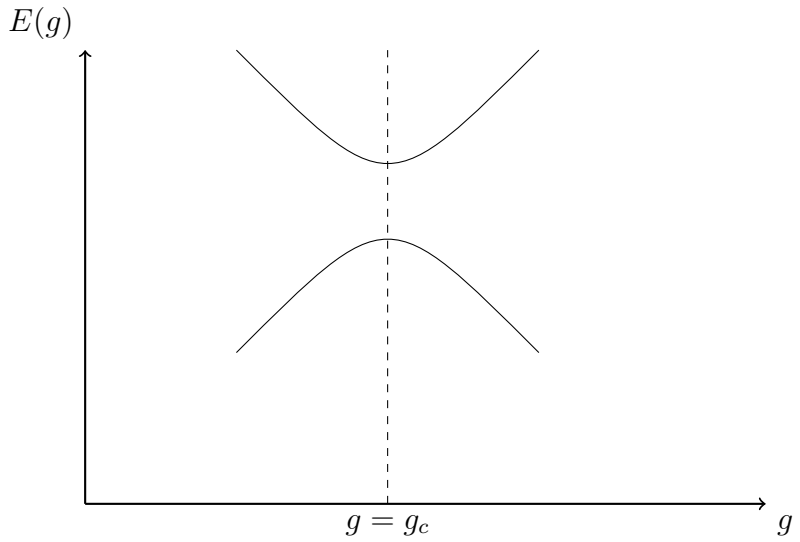

Source: the author (2022).

The Hamiltonian need not necessarily have the form $H(g) = H_0 + gH_1$, this was only used to set an example. Some systems not in thermodynamic limit can present the energy level structure of the avoided level crossing (figure 13), where the energy levels don't cross but come close to at value $g = g_c$ (SACHDEV, 2011). Since energy is extensive, the gap between the energy curves of an avoided level crossing will tend to zero as the system's size grows. In the thermodynamic limit, the avoided level crossing will tend to display a level cross at the value $g = g_c$ and the ground state will change. Again, the system will move to this new ground state when $g > g_c$.

Quantum phase transitions induced by magnetic fields in alternating spin chains were studied in this project. Spin-interacting systems are a known class of systems that can undergo quantum phase transitions. Mixed-spin Heisenberg chains can exist in varied quantum phases, as seen in (TENÓRIO; MONTENEGRO-FILHO; COUTINHO-FILHO, 2011).

4 DENSITY MATRIX RENORMALIZATION GROUP (DMRG)

In order to determine values of h_B that increase the magnetization of the lattice, it is necessary to calculate the energy levels $E_0(S^z)$. The interest will lie in the lowest energy eigenvalues $E_0(S^z)$ for each total S^z level so that the magnetization curve can be plotted using equations (2.26) and (2.27). This section will focus on elaborating the fundamentals of the numerical method known as Density Matrix Renormalization Group (or DMRG) (WHITE, 1992; WHITE, 1993), which allows us, through truncation, to reduce the dimension of the Hilbert space and evaluate the eigenvalues of energy of H_0 of one-dimensional chains (SCHOLLWÖCK, 2005). This is an important process, given the increasing difficulty of an exact diagonalization as the lattices become bigger.

4.1 DENSITY MATRIX

The density matrix operator is a fundamental part of the DMRG method and will have its formulation done in this section. Consider that a system is formed by an ensemble of pure states (mixture of states) $|\alpha^i\rangle$ with probability α^i. Define the density probability operator ρ as

$$\rho = \sum_i \alpha^i \left|\alpha^i\right\rangle \left\langle\alpha^i\right|. \tag{4.1}$$

The states $|\alpha^i\rangle$ are not necessarily orthonormal, so $\langle\alpha^i|\alpha^j\rangle$ is not necessarily equal to δ_{ij}. However, $\langle\alpha^i|\alpha^i\rangle = 1$.

Consider a generic basis represented by vectors $|b_i\rangle$. Then

$$I = \sum_i \left|b_i\right\rangle \left\langle b_i\right|. \tag{4.2}$$

I is the identity operator. Let A be an observable and $\langle A\rangle$ its average value. For the system described by ρ, $\langle A\rangle$ is given by the relation

$$\langle A\rangle = \sum_i \alpha^i \left\langle\alpha^i\right| A \left|\alpha^i\right\rangle. \tag{4.3}$$

Rewriting (4.3) using, it is valid that (4.2)

$$\langle A\rangle = \sum_i \alpha^i \left\langle\alpha^i\right| A \left|\alpha^i\right\rangle = \sum_{i,j,k} \alpha^i \left\langle\alpha^i|b_j\right\rangle \left\langle b_j\right| A \left|b_k\right\rangle \left\langle b_k|\alpha^i\right\rangle;$$

$$\langle A\rangle = \sum_{j,k} \underbrace{A_{jk}}_{\langle b_j|A|b_k\rangle} \underbrace{\langle b_k| \left(\sum_i \alpha^i \left|\alpha^i\right\rangle \left\langle\alpha^i\right|\right) |b_j\rangle}_{\rho_{kj}} = \sum_{j,k} A_{jk}\rho_{kj};$$

$$\langle A\rangle = \mathrm{Tr}\,(\rho A). \tag{4.4}$$

Naturally, $\sum_i w_i = 1$, so $Tr(\rho) = 1$. If the system is described by a pure state, a state vector $|\psi\rangle$ can be attributed, and the density matrix is reduced to $\rho = |\psi\rangle\langle\psi|$, and $\rho^2 = |\psi\rangle\langle\psi|\psi\rangle\langle\psi| = |\psi\rangle\langle\psi| = \rho$. A pure state is given by

$$\rho^2 = \rho = |\psi\rangle\langle\psi|\,. \tag{4.5}$$

4.1.1 Diagonalization of the density matrix

The density operator is Hermitian, with

$$\rho^\dagger = \sum_i \alpha^{i*} \left|\alpha^i\right\rangle \left\langle\alpha^i\right| = \sum_i \alpha^i \left|\alpha^i\right\rangle \left\langle\alpha^i\right|.$$

The density operator can be diagonalized on some basis with real eigenvalues. Such basis is here represented by the vectors $|w_i\rangle$, with $\rho\,|w_i\rangle = w_i\,|w_i\rangle$. It will be convenient sort w_i in the form $w_1 > w_2 > w_3 > ... > w_n$, with n the Hilbert space dimension. Unlike in section 4.1, where kets $|\alpha^i\rangle$ were not necessarily orthonormal, here, orthonormality is valid: $\langle w_i|w_j\rangle = \delta_{ij}$.

Since $|w_i\rangle$ is a basis, equation (4.2) is valid with $|b_i\rangle \to |w_i\rangle$. Using the identity $\rho I = \rho$, it is valid that

$$\rho I = \sum_i \rho\,|w_i\rangle\langle w_i| = \sum_i w_i\,|w_i\rangle\langle w_i|\,;$$

$$\rho = \sum_i w_i\,|w_i\rangle\langle w_i|\,. \tag{4.6}$$

Comparing equation (4.1) and (4.6), the system has a probability w_i to be found in the state $|w_i\rangle$.

4.2 REDUCED DENSITY MATRIX

Consider a subsystem A in contact with a subsystem B. Subsystem A has for a basis of Hilbert space the vectors $|i\rangle$, while subsystem B has as its basis the vectors $|j\rangle$. A state ket $|\psi\rangle$ for this combination will be given by

$$|\psi\rangle = \sum_{i,j} C_{ij} \, |i,j\rangle \, . \tag{4.7}$$

The state bra $\langle\psi|$ is given then by

$$\langle\psi| = \sum_{i',j'} C^*_{i'j'} \, \langle i',j'| \, . \tag{4.8}$$

The density matrix of the composite the system ρ^{Comp} is given by

$$\rho^{Comp} = \sum_{i,i',j,j'} C_{ij} C^*_{i'j'} \, |i,j\rangle \, \langle i',j'| \, . \tag{4.9}$$

There is a density matrix associated with each subsystem, known as the reduced density matrix. Those matrices will be represented by ρ^{A} for subsystem A and ρ^{B} for subsystem B. In order to obtain each, it is necessary to use the partial trace, defined as

$$\mathrm{Tr}_{\,A}(|A_1,B_1\rangle \, \langle A_2,B_2|) = |B_1\rangle \, \langle B_2| \, \mathrm{Tr} \, (|A_1\rangle \, \langle A_2|); \tag{4.10}$$

$$\mathrm{Tr}_{\,B}(|A_1,B_1\rangle \, \langle A_2,B_2|) = |A_1\rangle \, \langle A_2| \, \mathrm{Tr} \, (|B_1\rangle \, \langle B_2|). \tag{4.11}$$

It will be demonstrated how the partial trace is used to determine the reduced density matrices. A composite system formed by an ensemble of pure states $|i,j\rangle$ with probabilities w_{ij}, in which w_{ij} is the probability of simultaneously having subsystem A in state i and subsystem B in state j, while $\sum_j w_{ij}$ is the probability that system A is in state i, regardless of the state of subsystem B. The density matrix for subsystem A will then be given by

$$\rho^A = \sum_i \left(\sum_j w_{ij} \right) |i\rangle \, \langle i| \, . \tag{4.12}$$

The density matrix of subsystem B has an analogous form and is given by

$$\rho^B = \sum_j \left(\sum_i w_{ij} \right) |j\rangle \, \langle j| \, . \tag{4.13}$$

The composite density matrix is equal to

$$\rho^{Comp} = \sum_{i,j} w_{ij} \left|i,j\right\rangle \left\langle i,j\right| . \tag{4.14}$$

Applying partial trace in equation (4.14), one will find that

$$\mathrm{Tr}\,_A \rho^{Comp} = \sum_{i,j} w_{ij} \left|j\right\rangle \left\langle j\right| \underbrace{Tr(\left|i\right\rangle \left\langle i\right|)}_{=1};$$

$$\mathrm{Tr}\,_B \rho^{Comp} = \sum_{i,j} w_{ij} \left|i\right\rangle \left\langle i\right| \underbrace{Tr(\left|j\right\rangle \left\langle j\right|)}_{=1}.$$

Then, it is valid that

$$\mathrm{Tr}\,_A \rho^{Comp} = \sum_{i,j} w_{ij} \left|j\right\rangle \left\langle j\right| = \rho^B; \tag{4.15}$$

$$\mathrm{Tr}\,_B \rho^{Comp} = \sum_{i,j} w_{ij} \left|i\right\rangle \left\langle i\right| = \rho^A. \tag{4.16}$$

The reduced density matrix of each subsystem is then obtained using the partial trace, such that

$$\rho^{\mathsf{A}} = \mathrm{Tr}\,_B \rho^{Comp}; \tag{4.17}$$

$$\rho^{\mathsf{B}} = \mathrm{Tr}\,_A \rho^{Comp}. \tag{4.18}$$

Equations (4.17) and (4.18) result in

$$\rho^A = \sum_{i,i',j,j'} C_{ij} C^*_{i'j'} \left|i\right\rangle \left\langle i'\right| \mathrm{Tr}\left(\left|j\right\rangle \left\langle j'\right|\right); \tag{4.19}$$

$$\rho^B = \sum_{i,i',j,j'} C_{ij} C^*_{i'j'} \left|j\right\rangle \left\langle j'\right| \mathrm{Tr}\left(\left|i\right\rangle \left\langle i'\right|\right). \tag{4.20}$$

Now, using the relations $\mathrm{Tr}\left(\left|i\right\rangle \left\langle i'\right|\right) = \delta_{ii'}$ and $\mathrm{Tr}\left(\left|j\right\rangle \left\langle j'\right|\right) = \delta_{jj'}$, one will find that

$$\rho^A = \sum_{i,i',j} C_{ij} C^*_{i'j} \left|i\right\rangle \left\langle i'\right| ; \tag{4.21}$$

$$\rho^B = \sum_{i,j,j'} C_{ij} C^*_{ij'} \left|j\right\rangle \left\langle j'\right| . \tag{4.22}$$

Finally, defining $\rho^A_{ii'} = \langle i| \rho^A |i'\rangle$ and $\rho^B_{jj'} = \langle j| \rho^B |j'\rangle$, it is valid that

$$\rho^A_{ii'} = \sum_j C_{ij} C^*_{i'j}; \tag{4.23}$$

$$\rho^B_{jj'} = \sum_i C_{ij} C^*_{ij'}. \tag{4.24}$$

4.3 BLOCK, ENLARGED BLOCK, AND SUPERBLOCK

Consider a chain with L unit cells. A block $B(l_A, m_A)$ containing l_A unit cells ($l_A \leq L$) and m_A as its Hilbert space dimension are next to a single unit cell (figure 14), configuring an enlarged block.

Figura 14 – Block of l_A unit cells and a single unit cell. Enlarged block.

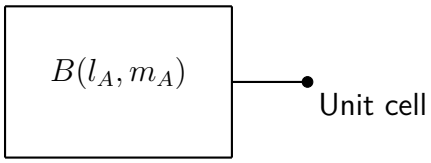

Source: the author (2022).

N_c will denote the Hilbert space dimension of a single unit cell, then the combination block + unit cell, here called enlarged block, will have dimension $N^A_{en} = m_A N_c > m_A$. Adding a unit cell to the block increased the Hilbert space dimension.

The question that drives the DMRG method is the following: how can the dimension of the enlarged block be reduced back to m_A maintaining precision? In order to progress and answer this question, consider subsystem A corresponding to the enlarged block surrounded by subsystem B, another identical enlarged block, forming a superblock (figure 15). This structure will be at the epicenter of the DMRG formulation.

Figura 15 – Superblock formed by combining two enlarged blocks: subsystem A (block $B(l_A, m_A)+$ unit cell) and subsystem B (block $B(l_B, m_B)+$ unit cell).

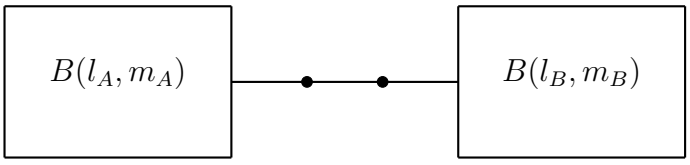

Source: the author (2022).

4.4 SUPERBLOCK STATE KET AND BRA; DENSITY MATRIX OPERATOR

The block's $B(l_A, m_A)$ basis will be denoted by $|m_{bA}\rangle$, with $m_{bA} = 1, 2, 3, ..., m_A$. Similarly, for the block $B(l_B, m_B)$, its basis will be denoted by $|m_{bB}\rangle$, with $m_{bB} = 1, 2, 3, ..., m_B$. As for the unit cells, their states will be represented $|n_{cA}\rangle$ for the site next to $B(l_A, m_A)$, and $|n_{cB}\rangle$ for the site next to $B(l_B, m_B)$, with $n_{cA} = 1, 2, 3, ..., N_c$ and the same goes for n_{cB}. Hence, a superblock's state ket ψ can be written as

$$|\psi\rangle = \sum_{m_{bA}} \sum_{n_{cA}} \sum_{m_{bB}} \sum_{n_{cB}} C_{m_{bA} n_{cA} m_{bB} n_{cB}} |m_{bA}\rangle |n_{cA}\rangle |m_{bB}\rangle |n_{cB}\rangle . \tag{4.25}$$

The tensor product $|m_{bA}\rangle |n_{cA}\rangle |m_{bB}\rangle |n_{cB}\rangle$ can be written as

$$|m_{bA}\rangle |n_{cA}\rangle |m_{bB}\rangle |n_{cB}\rangle = |m_{bA}, n_{cA}; m_{bB}, n_{cB}\rangle . \tag{4.26}$$

The values of $C_{m_{bA} n_{cA} m_{bB} n_{cB}}$ are determined using orthonormality, that is

$$\langle m_{bA}, n_{cA}; m_{bB}, n_{cB} | m'_{bA}, n'_{cA}; m'_{bB}, n'_{cB}\rangle = \delta_{m_{bB} m'_{bA}} \delta_{n_{cA} n'_{cA}} \delta_{m_{bB} m'_{bB}} \delta_{n_{cB} n'_{cB}}; \tag{4.27}$$

$$C_{m_{bA} n_{cA} m_{bB} n_{cB}} = \langle m_{bA}, n_{cA}; m_{bB}, n_{cB} | \psi\rangle . \tag{4.28}$$

Dual conjugation of (4.25) is given by

$$\langle\psi| = \sum_{m'_{bA}} \sum_{n'_{cA}} \sum_{m'_{bB}} \sum_{n'_{cB}} C^*_{m'_{bA} n'_{cA} m'_{bB} n'_{cB}} \langle n'_{cB}| \langle m'_{bB}| \langle n'_{cA}| \langle m'_{bA}| . \tag{4.29}$$

Equation (4.26) can be written in the form

$$|m_{bA}, n_{cA}; m_{bB}, n_{cB}\rangle = |i\rangle |j\rangle = |i, j\rangle . \tag{4.30}$$

Rewriting (4.25) and (4.29), it is valid that

$$|\psi\rangle = \sum_{i=1}^{N^A_{en}} \sum_{j=1}^{N^B_{en}} C_{ij} |i, j\rangle; \tag{4.31}$$

$$\langle\psi| = \sum_{i'=1}^{N^A_{en}} \sum_{j'=1}^{N^B_{en}} C^*_{i'j'} \langle i', j'|. \tag{4.32}$$

At this point, one may recall the subsection (4.2). The reduced density matrix ρ^{A} for the subsystem A (enlarged block $B(l_A + 1, N^{\mathsf{A}}{}_{en})$) is given using equation (4.23).

4.5 THE TRUNCATION PROCESS

Consider the two enlarged blocks forming a superblock of section 4.3, each with Hilbert space dimensions $d_A = N_{en}^A$ and $d_B = N_{en}^B$, respectively. The superblock has a Hamiltonian $H_0(l_A+1, N_{en}^A; l_B+1, N_{en}^B)$ and Hilbert space dimension equal $d = N_{en}^A N_{en}^B$. The Hamiltonian is assumed to be practical to diagonalize using any available method.

From equation (2.9), the eigenstates of Hamiltonian are eigenstates of S^z (total angular momentum in z direction). The interest will lie in studying the lowest energy states $|\psi\rangle$ for each value of total S^z. The states $|\psi\rangle$ will have coefficients in the form of equation (4.31) and the reduced density matrix ρ can be obtained from (4.23).

Diagonalization of ρ will lead to equation (4.6), with w_i the probability of the system existing in the pure state $|w_i\rangle$. So, when w_i is small, there is a low probability that the system will be found in the pure state $|w_i\rangle$, hence the argument to truncation: it is possible, at cost of accuracy, to truncate the Hilbert space by keeping only the most probable states (states with higher values of w_i).

4.5.1 The infinite DMRG process

The infinite DMRG infinite process consists of increasing system sizes while maintaining a Hilbert space dimension lower than the defined max number. Here, it will be considered that the maximum Hilbert space dimension is m_A.

The steps on how to proceed with DMRG to perform truncation for an infinite-size chain are listed below:

1. From a block $B(l_A, m_A)$, form an enlarged block $B(l_A + 1, N_{en}^A)$ by adding a unit cell. This enlarged block will have an environment of the same size $B(l_A + 1, N_{en}^A)$. The combination of the two enlarged blocks is the superblock. It is assumed that it is practical to diagonalize the Hamiltonian of this superblock.

2. Obtain the lowest energy states for each possible total S^z. From the eigenstates $|\psi\rangle$, with coefficients given by equation (4.28), determine the reduced density matrix ρ for block $B(l_a + 1, N_{en}^A)$ using equation (4.23).

3. Diagonalize ρ and find the probabilities w_i. Sort the vectors $|w_i\rangle$ in a way so that the probabilities are ordered: $w_1 > w_2 > ... > w_{N_{en}^A}$. The initial block $B(l_A, m_A)$ had its Hilbert space dimension given by m_A. When a unitary cell was added to the block, the dimension increased to $N_{en}^A = m_A N_c$.

4. Perform the truncation: the eigenstates of $|w_i\rangle$ (that constitute a basis), once spammed from $i = 1$ to $i = N_{en}^A = m_A N_c$ will now spam from $i = 1$ to $i = m_A$. This corresponds to discarding the least probable states, and a reduction of the number of vectors in the basis. The result: the Hilbert space dimension was reduced back to the original size m_A, even though it has been added a unit cell to the block.

5. Return to step 1, but with a block $B(l_A+1, m_A)$, with l_A+1 corresponding to a unit cell added. Note that the dimension m_A has remained unchanged, thanks to the truncation process.

6. The process is to be repeated until the energies per unit cell converge.

4.5.2 The finite DMRG process

The finite process seeks to evaluate a finite system with L unit cells. It ends up having more precision than the infinite process. For simplicity, one should look to use always even sizes. This process starts as the infinite process, forming a block with 1 unit cell, proceeding to an enlarged block of 2 unit cells, and forming a superblock with 4 unit cells. The infinite process steps are followed until the superblock has size L, with the maximum Hilbert space dimension allowed given by m_A. From this point, the algorithm starts to perform sweeps. There are two blocks with the same size, given by $\frac{L}{2}$, one on the right, and another on the left.

The sweeping process consists of enlarging one block by a unit cell, while decreasing the other block size, maintaining the number of unit cells constant at L. Starting by increasing the block on the left, the superblock Hamiltonian is evaluated, the eigenstates of energy are established, the density operator of the superblock is obtained, the reduced density matrix of the left block is determined, truncation (if necessary) is performed, and the process follows up to the point that the right block has a single unit cell. This counts as one sweep. From this point, the right block is enlarged while the left block is decreased in an identical process until the left block is left with just one unit cell. The finite process consists of a repetition

of the sweeping process by a determined number of sweeps. The DMRG algorithm used in this dissertation is the one provided by the Algorithms and Libraries for Physics Simulations (ALPS) project (BAUER et al., 2011).

4.6 DISCARDED WEIGHT

An important measure of the accuracy while performing the DMRG method is the discarded weight ϵ. In the $|w_i\rangle$ basis the reduced density matrix is equal to

$$\rho = \sum_{i=1}^{N_{en}^{s}} w_i \left|w_i\right\rangle \left\langle w_i\right| .$$

Since $Tr(\rho) = 1$, it is valid that

$$\sum_{i=1}^{N_{en}^{A}} w_i = 1. \tag{4.33}$$

Equation (4.33) can be broken down into the two summations

$$\sum_{i=1}^{N_{en}^{A}} w_i = \sum_{i=1}^{m_A} w_i + \sum_{i=m_A+1}^{N_{en}^{A}} w_i = 1. \tag{4.34}$$

Define discarded weight ϵ as

$$\epsilon = \sum_{i=m_A+1}^{N_{en}^{A}} w_i = 1 - \sum_{i=1}^{m_A} w_i. \tag{4.35}$$

In order to maintain precision, ϵ is required to be as small as possible. It is a measure of how different the approximate result will be from the real result. For a qualitative demonstration, consider a generic observable A and its real average value $\langle A\rangle$. It is valid that

$$\langle A\rangle = \sum_{i=1}^{N_{en}^{A}} w_i \left\langle w_i\right| A \left|w_i\right\rangle ;$$

$$\langle A\rangle = \sum_{i=1}^{m_A} w_i \left\langle w_i\right| A \left|w_i\right\rangle + \sum_{i=m_A+1}^{N_{en}^{A}} w_i \left\langle w_i\right| A \left|w_i\right\rangle .$$

Truncating, the approximate value $\langle A\rangle_{aprox}$ is equal to

$$\langle A\rangle_{aprox} = \sum_{i=1}^{m_A} w_i \left\langle w_i\right| A \left|w_i\right\rangle . \tag{4.36}$$

Then, the difference between the real value $\langle A \rangle$ and the approximate value $\langle A \rangle_{aprox}$ is given by

$$\langle A \rangle - \langle A \rangle_{aprox} = \sum_{i=m_A+1}^{N_{en}^A} w_i \langle w_i | A | w_i \rangle . \tag{4.37}$$

Let A_{max} represent the maximum positive value of $\langle w_i | A | w_i \rangle$. Then, it is valid that

$$| \langle A \rangle - \langle A \rangle_{aprox} | \leqslant \sum_{i=m_A+1}^{N_{en}^A} w_i A_{max} = A_{max} \epsilon. \tag{4.38}$$

Ultimately, the error associated with the DMRG process is bound by the discarded weight ϵ. Implementing the DMRG algorithm to obtain the energy levels for each total S^z, the truncated error did not exceed the magnitude of 10^{-10}.

4.7 DMRG PARAMETERS

The DMRG algorithm uses some parameters that can either augment its precision or decrease its running time. Such parameters are important in order to determine how the algorithm should run. They will be listed in this section for the sake of enlightenment.

The model of the simulation will be the spin model, which institutes the Heisenberg Hamiltonian with zero magnetic field ($h_B = 0$), which accounts for the interaction of spin between sites through the Hamiltonian. Also, it was demonstrated, the total S^z states are the eigenvalues of the Hamiltonian, and the DMRG can run for specific values of total S^z. This corresponds to diagonalizing the Hamiltonian at subspaces of total S^z. Since the chain's Hamiltonian eigenstates are also eigenstates of total S^z, the process of diagonalization can be done in any subspace of total S^z. Defining which subspace that is, the DMRG process will evaluate the lowest energy available for the specified S_z. Naturally, this process will be repeated until all available total S^z are covered.

Another variable of interest is the truncation error. In order to maintain precision, it is necessary to make sure this error is not high. The DMRG algorithm allows the user to choose the maximum truncation error allowed. However, it can be rather difficult to follow this path since, if chosen poorly, the error may exceed this maximum value for such chain size and the simulation will not run. An alternative is to choose the maximum number of states that are kept. Increasing this number lowers the number of states that are discarded when adding unit cells to the block, as described in the previous sections. As the number of states kept

increases, it is expected that the truncation error decreases. In the scope of this text, it was set that the maximum number of states kept was 240. This refers to the maximum Hilbert space dimension allowed throughout the iteration process while covering the entire chain. Once the number of basis vectors surpasses the defined max states number, the truncation process must be done in order to reestablish the maximum value allowed. It was observed that the truncation error did not exceed the magnitude of 10^{-10}, which can be argued to be very low, confirming a good choice of max states kept. The downside, however, is that the algorithm becomes computationally demanding, taking more time to run. The number of sweeps in the finite DMRG process was chosen to be 8.

4.8 EXAMPLES OF DMRG APPLICATION

In order to be sure the DMRG is accurate, it was used to obtain the results for known spin models. Three types of chains were tested: the antiferromagnetic spin $\frac{1}{2}$ ladder, the open spin-$\frac{1}{2}$ and the open spin-1 chains. The spin-$\frac{1}{2}$ chain will be seen to have no magnetization gap, while the spin-1 and the antiferromagnetic ladder do, in agreement with articles on condensed matter physics. For each type of chain, it will be shown the energy levels $E_0(S^z)$ obtained at zero magnetic field using the DMRG algorithm. This energy curve is used to obtain the magnetization as a function of an applied magnetic field.

Of course, the curves have a dependency on the chain size L. As the size increases, the levels of energy are expected to grow, since, with more spin, there will be more interaction terms. However, it is expected that the energy difference between levels will not increase, only fluctuate, but overall remain comparable. With that in mind, it is convenient to plot the energy levels normalized by the chain size and plot the total magnetization per unit cell. Since the magnetic field measure h_B depends on the energy difference between levels, it will also fluctuate for different sizes of chain. Although the major interest would lie in the thermodynamic limit, where $L \to \infty$, this section seeks only to evaluate the results provided by the DMRG algorithm. For that purpose, a single value for the chain size will suffice. However, in the results section, it will be necessary to vary the chain size in order to investigate how the physical properties would behave in thermodynamic limit.

4.8.1 Open spin-$\frac{1}{2}$ chain

The one-dimensional spin-$\frac{1}{2}$ chain is one of the simplest forms of magnetic chains. Its energy curve has no energy degeneracy or sharp points (figure 16). Instead, the energy simply grows with the total magnetization, an expected behavior for a material with antiferromagnetic coupling. For an antiferromagnetic coupling, the lowest energy state would be all sites counter-aligned, making the total $S = 0$ the ground state. The ground state energy found of -0.44 is in agreement with the value shown at (WHITE, 1992). At zero temperature, the chain will have this magnetization. As the magnetic field increases, the levels with higher S^z will lower their energies, and the magnetization will start to grow since these S^z become energetically accessible. With no sharp points, the energy curve leads to a magnetization curve with just one plateau: the saturation plateau (figure 17). The curve has no magnetization jump, and the magnetization simply increases with the magnetic field.

The lack of a magnetization plateau means there is no energy gap between the ground state and the first excited state (i.e. the Hamiltonian is gapless). The fact that a half-integer spin chain is gapless is in accordance with Haldane's conjecture. Haldane argued that integer spin chains will be gapped, while half-integer spin chains will be gapless (HALDANE, 1983a; HALDANE, 1983b; AFFLECK; LIEB, 1986; AFFLECK, 1990; WAMER et al., 2020).

The step form of figure 17 was anticipated. These steps will decrease with the size of the system, which leads to say that, in the thermodynamic limit, there is no magnetization plateau, except the saturation one. This will be a different result for the subsequent spin-1 and antiferromagnetic spin-$\frac{1}{2}$ ladder chains.

Figura 16 – Open spin-$\frac{1}{2}$ chain energy levels $E_0(S^z)$ with $h_B = 0$. The number of unit cells was $L = 80$, totaling 80 sites.

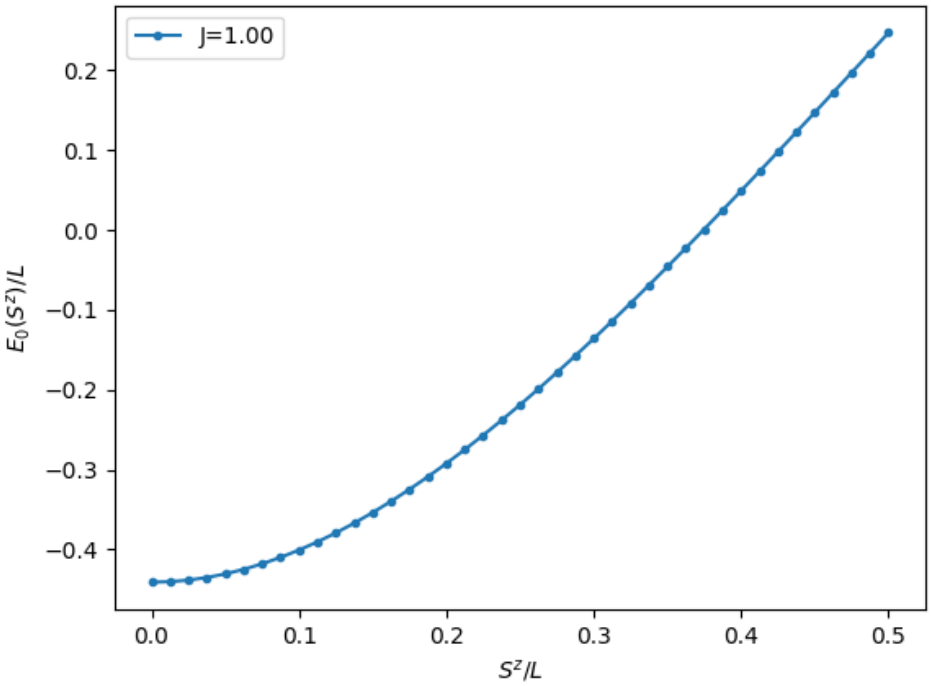

Source: the author (2022).

Figura 17 – Open spin-$\frac{1}{2}$ chain's magnetization per unit cell as a function of magnetic field h_B. Number of unit cells $L = 80$, totaling 80 sites.

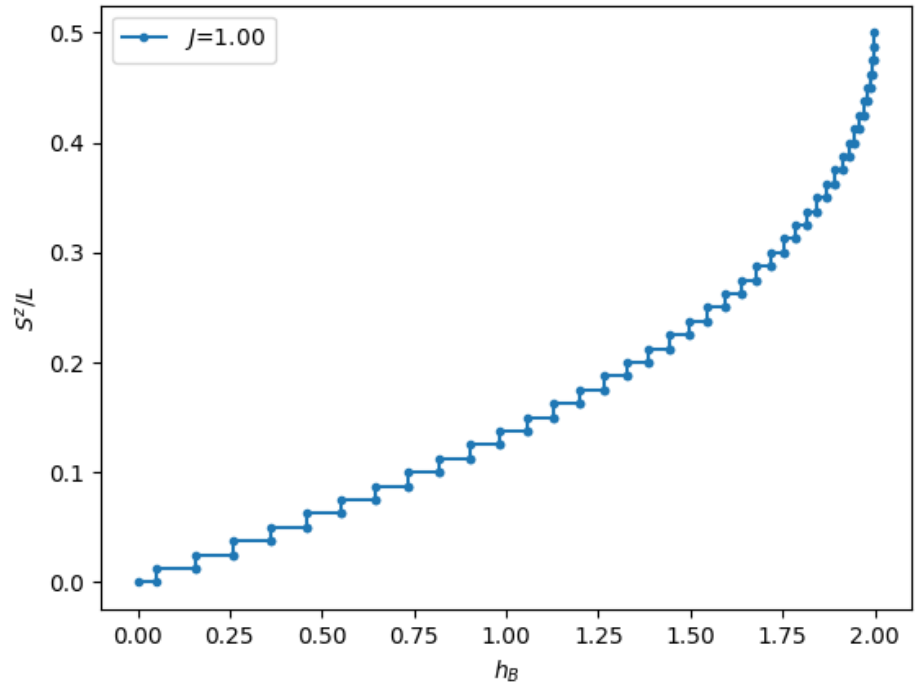

Source: the author (2022).

4.8.2 Open spin-1 chain

Like the open spin-$\frac{1}{2}$ chain, the open spin-1 chain is chain of spins. Its energy levels (figure 18) also grow with total magnetization. The ground state energy was also determined by White and the value of -1.4 is in agreement with (WHITE, 1992). It has a fundamental difference from the spin-$\frac{1}{2}$ case: its slope has a discontinuity. This will lead to a plateau in the magnetization curve (figure 19), since the slope abruptly changes its value from one point to another. The plateau size will be proportional to the coupling J between sites (JOLICOEUR; GOLINELLI, 2019).

Figura 18 – Open spin-1 chain energy levels $E_0(S^z)$ with $h_B = 0$. The number of unit cells was $L = 80$, totaling 80 sites.

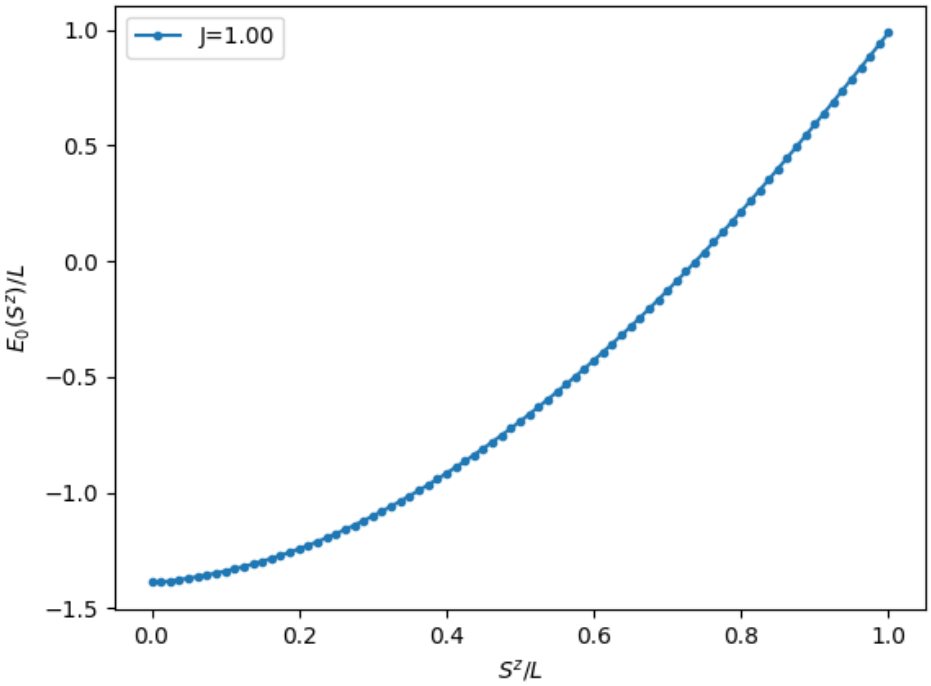

Source: the author (2022).

Figura 19 – Open spin-1 chain's magnetization per unit cell as a function of magnetic field h_B. Number of unit cells $L = 80$, totaling 80 sites.

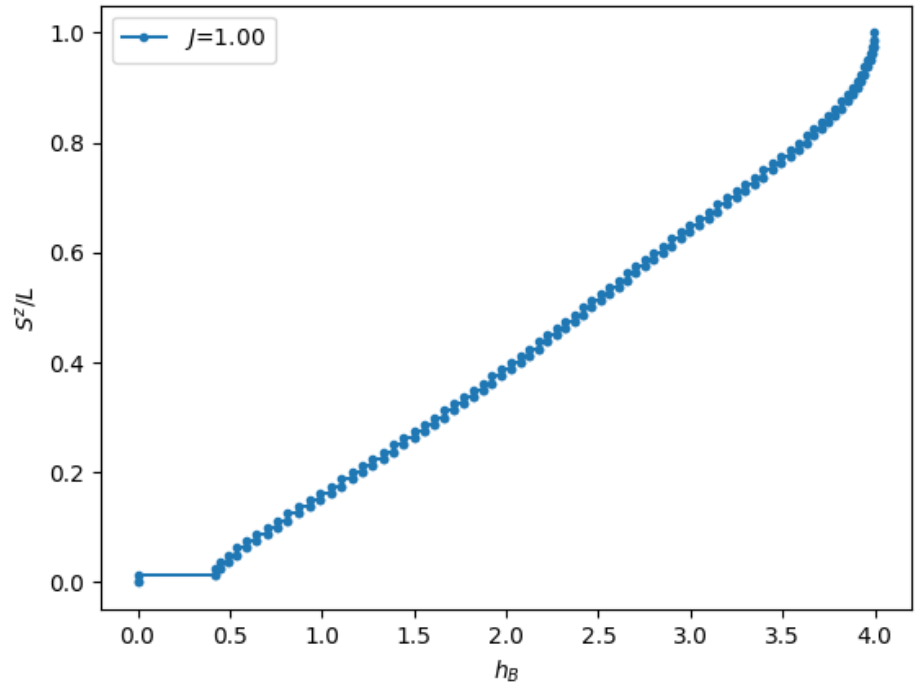

Source: the author (2022).

4.8.3 Antiferromagnetic spin-$\frac{1}{2}$ ladder

The antiferromagnetic spin-$\frac{1}{2}$ ladder will be described by the ladder unit cell (figure 8), with all sites having spin-$\frac{1}{2}$. The coupling J_0 will be maintained fixed at 1. The energy levels have the form depicted in figure 20. The ground state energies found are in agreement with the values shown at (BARNES et al., 1993). For instance, for $J_1 = 1$, figure 20 indicates a ground state with energy -0.575 per spin, in agreement with the value of -0.578 (ground state energy in the thermodynamic limit) shown in (BARNES et al., 1993). The magnetization curve (figure 21) will display a magnetization plateau for $J_1 \neq 0$ cases, with plateau size proportional to J_1.

Figura 20 – Antiferromagnetic spin-$\frac{1}{2}$ half ladder energy levels $E_0(S^z)$ with $h_B = 0$. The number of unit cells was $L = 20$, totaling 80 sites.

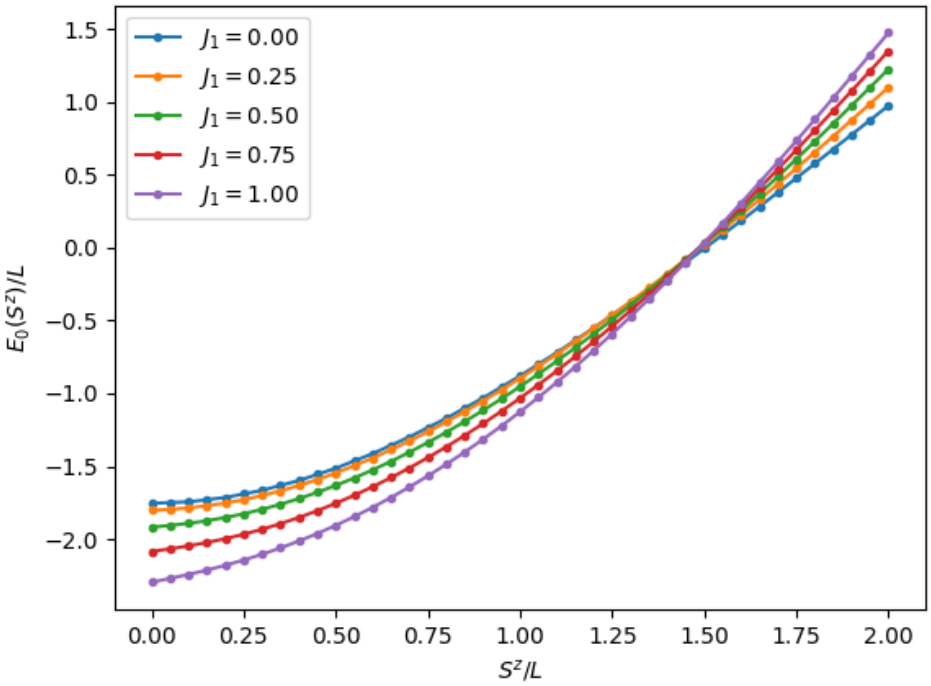

Source: the author (2022).

Figura 21 – Antiferromagnetic spin-$\frac{1}{2}$ ladder magnetization per unit cell as a function magnetic of the field h_B. Number of unit cells $L = 20$, totaling 80 sites. There is a plateau for the $J_1 \neq 0$ cases. The plateau size increases with the value of J_1.

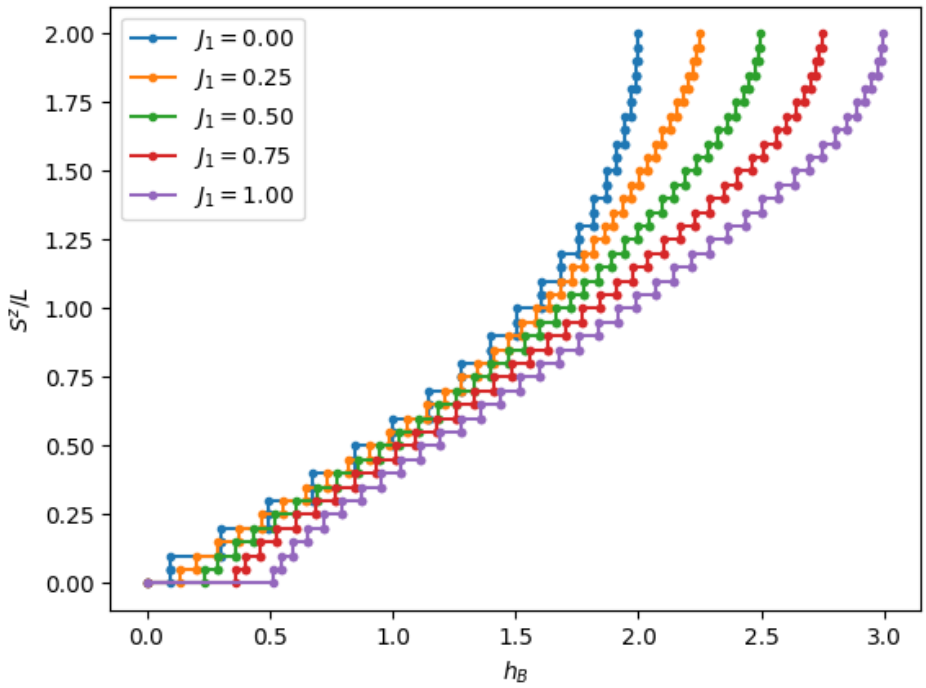

Source: the author (2022).

The ladder compounds are of ample interest throughout condensed matter physics research. The article (DAGOTTO; RICE, 1996) covers a variety of information on ladder compounds. For the antiferromagnetic spin-$\frac{1}{2}$ ladder, the magnetization curve has a plateau size of 0.5, approximately, which corresponds to a gap between the energy levels $E_0(0)$ and $E_0(1)$. This value is in agreement with the values shown at (DAGOTTO; RICE, 1996; BARNES et al., 1993), while (WHITE; NOACK; SCALAPINO, 1994) found the value of 0.504. The energy gap between levels $E_0(0)$ and $E_0(1)$ (evaluated in the thermodynamic limit) as a function of the coupling J_1 and J_0 can be seen at figure 22.

Figura 22 – Energy gap of the antiferromagnetic spin-$\frac{1}{2}$ ladder.

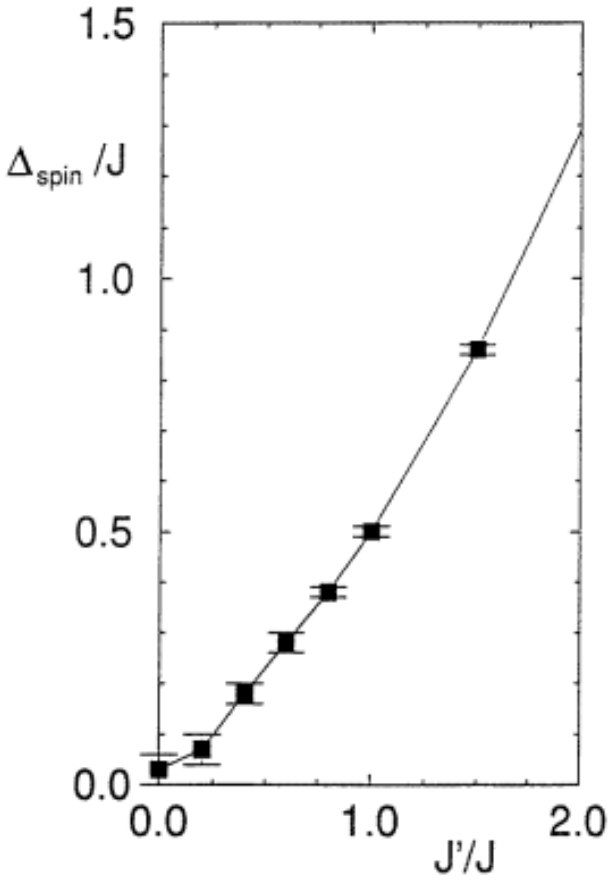

Source: (BARNES et al., 1993).

4.9 MIXED SPIN-1 AND SPIN-$\frac{1}{2}$ ANTIFERROMAGNETIC CHAIN

The mixed spin-1 and spin-$\frac{1}{2}$ chain can be described by the ladder unit cell (8) with $J_1 = 0$. By setting $J_1 = 0$ and $J_0 = 1$, there are two uncoupled chains with mixed spin-1 and spin-$\frac{1}{2}$. The energy curve (figure 23) has an energy gap, which leads to a magnetization plateau at the magnetization curve (figure 24).

Figura 23 – Mixed spin-1 and spin-$\frac{1}{2}$ chain energy levels $E_0(S^z)$ with $h_B = 0$. The number of unit cells was $L = 20$, totaling 80 sites.

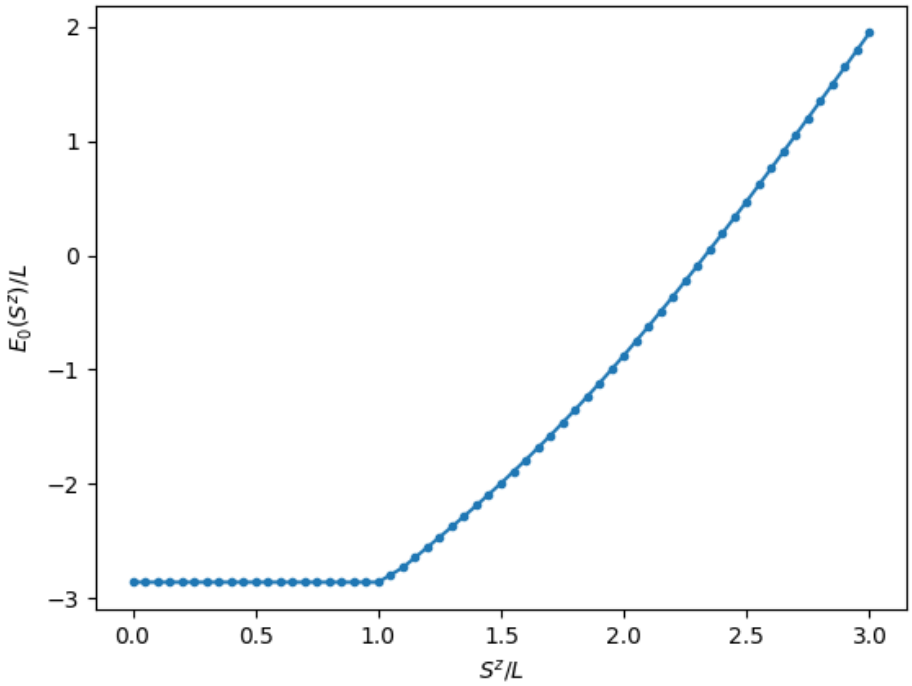

Source: the author (2022).

Figura 24 – Mixed spin-1 and spin-$\frac{1}{2}$ magnetization per unit cell as a function magnetic of the field h_B. Number of unit cells $L = 20$, totaling 80 sites.

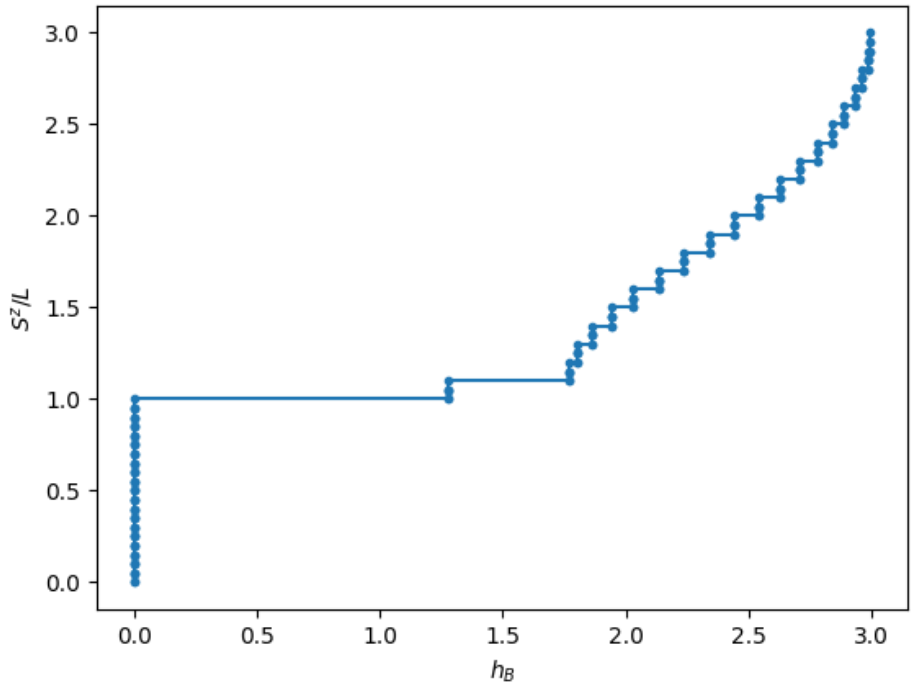

Source: the author (2022).

The ground state energy was found to be -2.87 per unit cell or -0.718 per site. This value is in agreement with the ground state energy shown at (PATI; RAMASESHA; SEN, 1997; BREHMER; MIKESKA; YAMAMOTO, 1997), obtained using spin-wave theory. It is also in agreement with the ground state energy shown at (KOLEZHUK; MIKESKA; YAMAMOTO, 1997), obtained using the quantum Monte Carlo (QMC) method.

There is an energy gap between the ground state and the first excited state. This gap had an approximate value of 1.78. Increasing the system size should lead to a closer gap value to the value of 1.759 shown at (MAISINGER et al., 1998).

5 MIXED SPIN-1 AND SPIN-$\frac{1}{2}$ LADDER UNDER A MAGNETIC FIELD

In this section, some physical properties of the mixed spin-1 and spin-$\frac{1}{2}$ ladder are investigated. In the first part, the chain has only antiferromagnetic couplings ($J_0 > 0$ and $J_1 > 0$), exhibiting ferrimagnetic order. The energy levels will be obtained using the DMRG algorithm, with the parameters described in section 4.7, and the maximum truncation error obtained is 10^{-10}. It is also considered the local magnetization and a comparison to the particle in a box wave function is done. Passing to a vertical ferromagnetic coupling ($J_1 < 0$), there is a change in many physical properties.

5.1 MIXED SPIN-1 AND SPIN-$\frac{1}{2}$ LADDER WITH ANTIFERROMAGNETIC COUPLINGS

For antiferromagnetic couplings, the ground state has a spin ordering with magnetization 1 per unit cell (figure 25). The energy levels $E_0(S^z)$ of the Heisenberg model H_0 under no magnetic field ($h_B = 0$) are a function of the total spin S and total S^z. The levels $E_0(S^z)$ presented at the plot (figure 26) are the lowest energy levels for each S^z at zero magnetic field ($h_B = 0$).

Figura 25 – Ground state ordering of the purely antiferromagnetic coupled ladder ($J_1 > 0$ and $J_0 > 0$). The total magnetization of this state corresponds to 1 per unit cell.

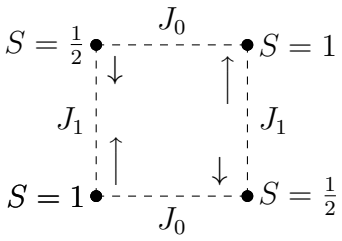

Source: the author (2022).

5.1.1 Energy levels $E_0(S^z)$ and magnetization curve

An important magnetization value of the ferrimagnetic ladder is the $\frac{1}{3}$ of saturation value. Since maximum magnetization of a unit cell corresponds to 3 (two spin-1 sites $+$ two spin-$\frac{1}{2}$ sites), the $\frac{1}{3}$ of the saturation value corresponds exactly to magnetization 1 per unit cell. The coupling J_0 will be maintained fixed at 1. The energy levels of the ferrimagnetic ladder (figure 26) present an energy degenerescence with S^z in the interval ranging from 0 to 1 per unit

cell (the $\frac{1}{3}$ saturation value). This means the chain can exhibit any S^z in this interval at zero temperature and zero magnetic field, since they are all in the same energy level. However, an arbitrarily small magnetic field would make the $S^z = 1$ per unit cell state the lowest energy state, since it has greater magnetization and greater downshift due to the Zeeman term.

The total $S^z > 1$ per unit cell states, however, are out of the energy degenerescence, and the energy levels have the same crescent tendency shown before. From this point, the S^z will grow with the magnetic field and the Hamiltonian is gapless.

In order to determine the S^z as a function of h_B, equations (2.26) and (2.27) are used to plot the magnetization curve and there is a sharp point at the energy level curve, which will naturally lead to a magnetization plateau in the magnetization curve (figure 27).

One may see that there are two magnetization plateau steps, with the second step getting smaller as J_1 increases. Increasing the chain size, the steps will have practically the same height, which results in one larger magnetization plateau in the thermodynamic limit. All the physical observables shown so far were obtained using a fixed lattice size and serve the purpose to give an insight into the properties of each spin model. However, in order to truly determine each physical observable, it is necessary to study the chains in the thermodynamic limit, in which the size would tend to infinity ($L \to \infty$). This is often achieved through the extrapolation of data obtained after running the DMRG for multiple chain sizes. In the following sections, there will be a discussion on how to extrapolate the data to the thermodynamic limit, where it will be evaluated the magnetization plateau size for this mixed spin-1 and spin-$\frac{1}{2}$ ladder.

Figura 26 – Ferrimagnetic ladder energy levels $E_0(S^z)$ with $h_B = 0$. The number of unit cells was $L = 20$, totaling 80 sites.

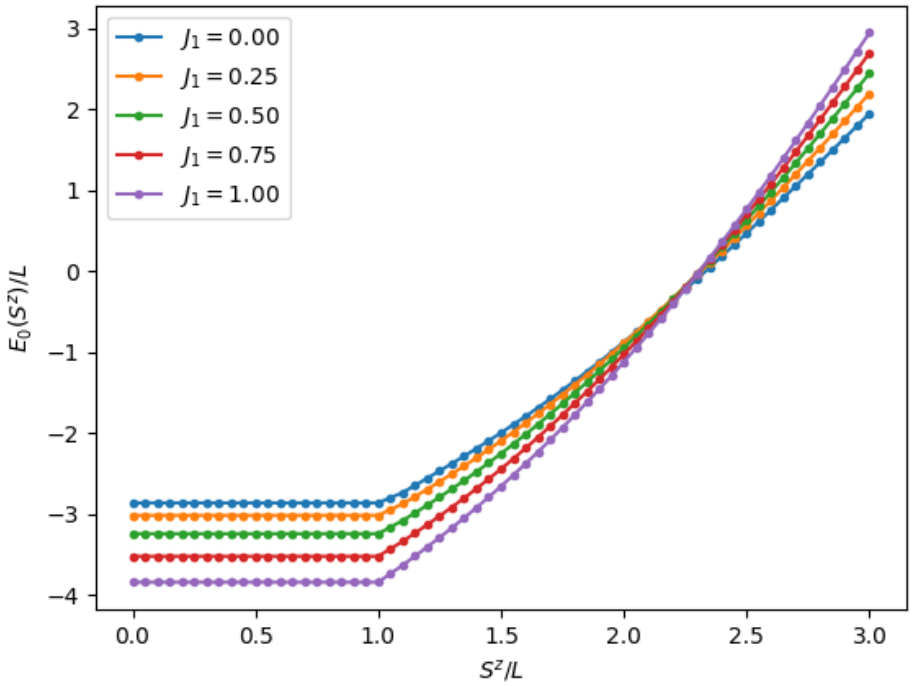

Source: the author (2022).

Figura 27 – Ferrimagnetic ladder magnetization per unit cell as a function of the magnetic field h_B. Number of unit cells $L = 20$, totaling 80 sites. Notice the magnetization plateau as in the spin one chain case.

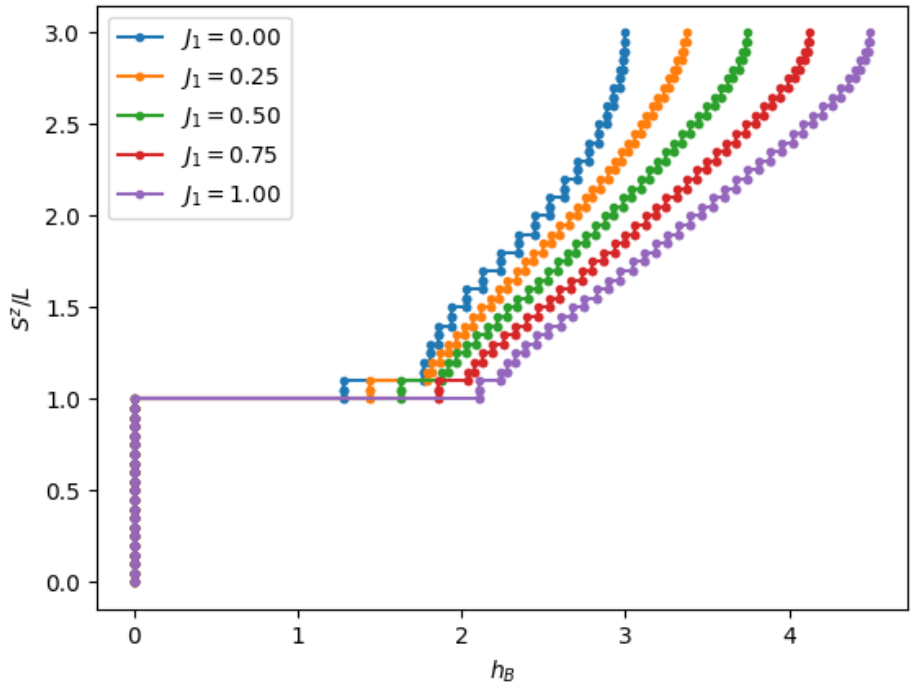

Source: the author (2022).

5.2 SPIN ORIENTATION OF THE FERRIMAGNETIC LADDER WITH SITES SPIN 1 AND $\frac{1}{2}$

The local spin variable is an average of the spin in the z direction throughout the chain. For each total S^z in the ket form $|s, m\rangle$, there is a linear combination in the basis $|m_1, m_2, ...\rangle$, with m_i the eigenvalue associated with the spin in the z direction of site i. It is valid that

$$m = \sum_i m_i.$$

One may recall the section where the Heisenberg dimer with mixed spin-1 and spin-$\frac{1}{2}$ was discussed. For instance, the state $|s = 1/2, m = 1/2\rangle$ was equivalent to

$$|s = 1/2, m = 1/2\rangle = \sqrt{\frac{1}{3}}\,|0, 1/2\rangle - \sqrt{\frac{2}{3}}\,|1, -1/2\rangle\,,$$

and there is a $1/3$ probability that the spin-$\frac{1}{2}$ site has for its z component of spin the $1/2$ value, and $2/3$ of probability of having the $-1/2$ value. Its z component of spin has averages

given by

$$\langle S_2^z \rangle = \frac{1}{3} \cdot \frac{1}{2} - \frac{2}{3} \cdot \frac{1}{2} = -\frac{1}{6},$$

with $\langle S_2^z \rangle$ standing for the average z component of spin for the site 2. In this notation, $\langle S_1^z \rangle$ would stand for the average value of the z component of spin for the site 1, which would be the spin-1 site. It follows directly that

$$\langle S_1^z \rangle = \frac{2}{3},$$

and the average of total spin $\langle S^z \rangle = \langle S_1^z + S_2^z \rangle$, such that

$$\langle S^z \rangle = \frac{4}{6} - \frac{1}{6} = \frac{1}{2},$$

as it should be.

The lowest energy level $E_0(S^z)$ of a total S^z state will have a ket that is a linear combination of the basis $|m_1, m_2, ...\rangle$, which provides for an average $\langle S_i^z \rangle$ for each site. This average is referenced as the local S^z.

For a mixed spin-1 and spin-$\frac{1}{2}$ chain with antiferromagnetic coupling, the local S^z throughout the chain for the total S^z given by $\frac{1}{3}$ of the saturation value has, except at the edges, a symmetric form (figure 28).

Figura 28 – Local S^z of the mixed spin-1 and spin-$\frac{1}{2}$ chain with antiferromagnetic coupling.

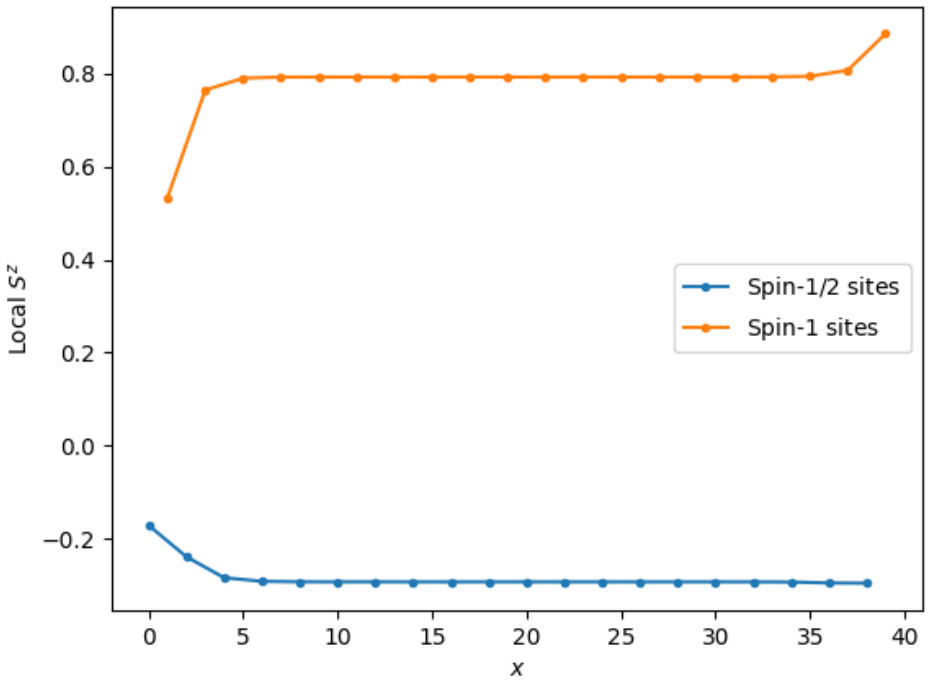

Source: the author (2022).

The ferrimagnetic ladder presents an energy degenerescence at zero magnetic field ($h_B = 0$): the $\frac{1}{3}$ magnetization plateau. For L unit cells, the saturation value of total S^z will be $3L$, and the $\frac{1}{3}$ of the saturation value would be just L. Here, it will be considered the case in which $J_0 = J_1 = 1$. Comparing the local S^z at the level of total S^z given by $\frac{1}{3}$ of the saturation value between the mixed-spin chain and the mixed-spin ladder, it can be argued that the ladder has (again, except at the edges) a more symmetric form (figure 29).

Figura 29 – Local S^z of the mixed-spin ladder. $J_0 = J_1 = 1$.

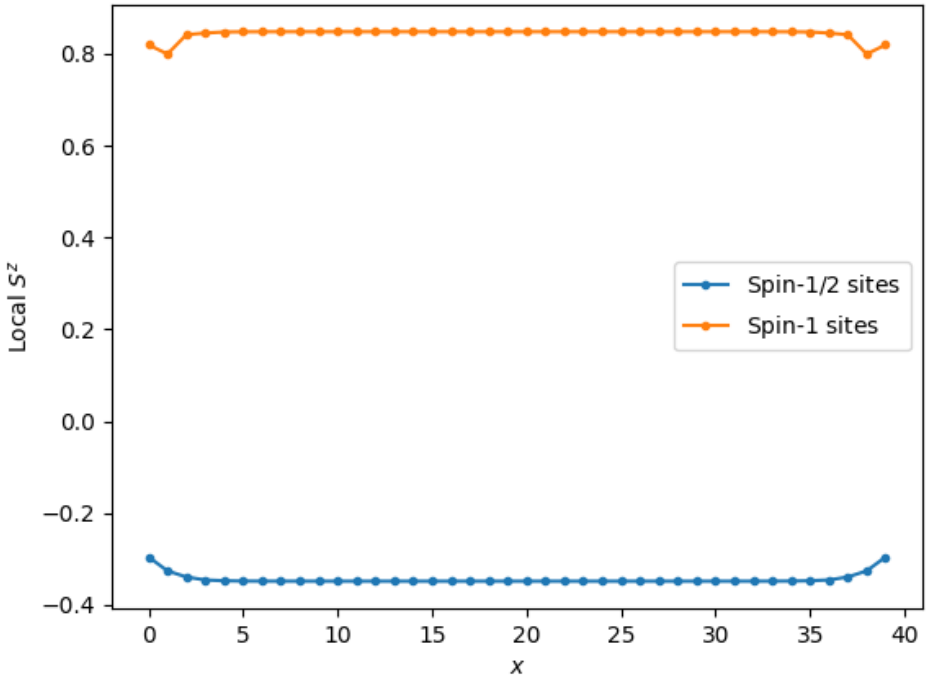

Source: the author (2022).

There is an interest in investigating the spin orientation of the chain's dimers for the values of total $S^z = L - 1$, L, $L + 1$, $L + 2$ and $L + 3$ (figure 30).

Figura 30 – Ferrimagnetic ladder average spin orientation for each dimer. The number of unit cells was $L = 20$, totaling 80 sites. $J_1 = J_0 = 1$.

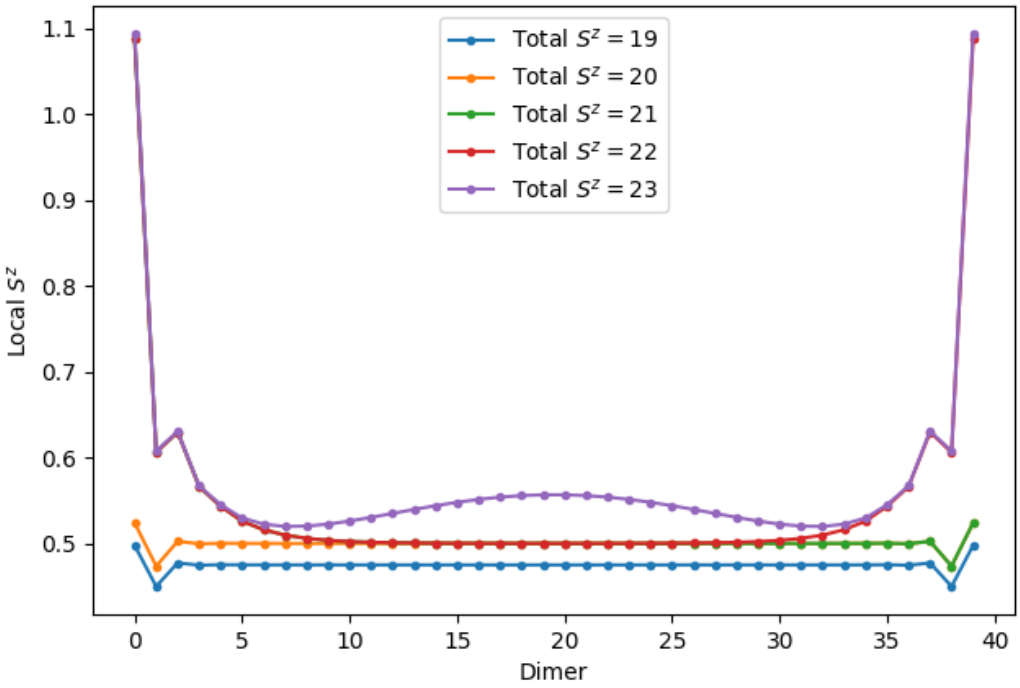

Source: the author (2022).

As total magnetization increases, the local spin of each dimer will increase as well. However, the increases occur first at the edges rather than the chain's interior. When S^z increases to the L value, the magnetization at the chain's interior starts to grow, and a comparison with the free particle confined to a potential well can be drawn. The difference of local magnetization between levels has an interesting format (figure 31), especially the difference of local S^z between the total S^z levels $L + 2$ and $L + 3$.

Figura 31 – Local S^z difference for different total S^z levels. $J_1 = J_0 = 1$.

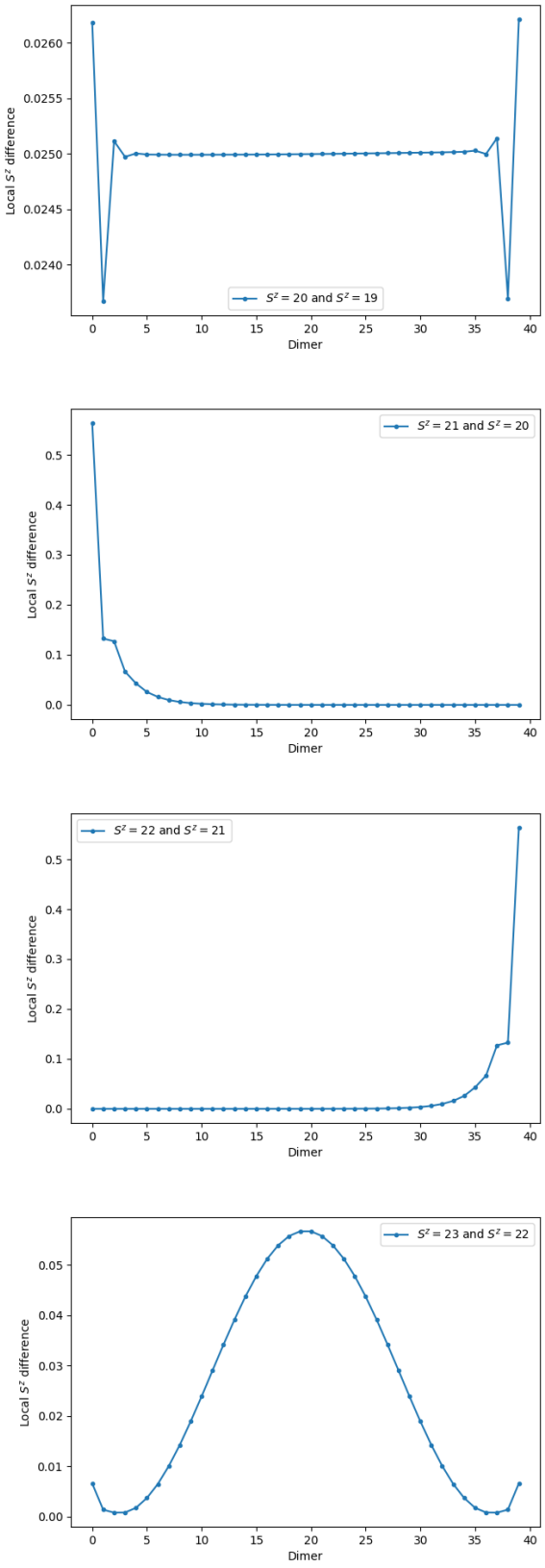

Source: the author (2022).

The summation of all points in any of the curves must be equal to 1 since this is the difference of total S^z between levels. As the chain increases, it can be argued that this summation extends to an integration process that equates to 1. All this construct resembles a wave function, with its quadratic integrated being equal to 1. The ground state wave function (normalized) of a particle with mass m_p confined in a box with length L_P is equal to

$$\psi_1(x) = \sqrt{\frac{2}{L_P}} \sin\left(\frac{\pi x}{L_p}\right). \tag{5.1}$$

The local S^z difference between S^z levels $L+3$ and $L+2$ is well fit by the wave function of equation (5.1) (figure 32).

Figura 32 – Quadratic ground state wave function with $L_p = 39$ (continuous line) and difference of local S^z between states of total $S^z = L+2$ and $S^z = L+3$ (dots).

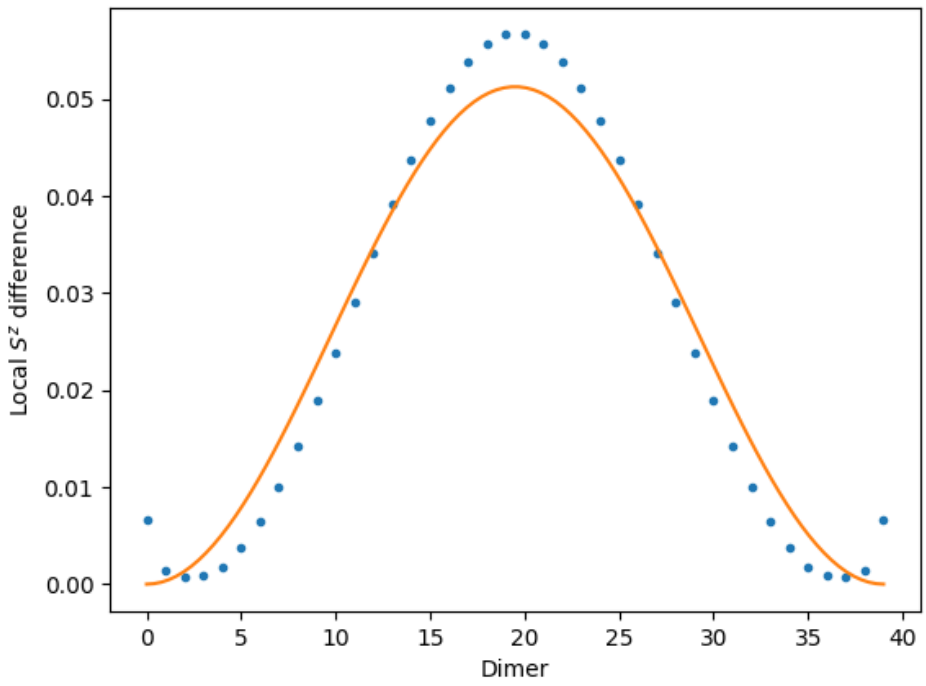

Source: the author (2022).

It can be concluded that the extra spin behaves as a particle confined to a unidimensional potential box.

5.3 MIXED SPIN-1 AND SPIN-$\frac{1}{2}$ LADDER WITH FERROMAGNETIC COUPLING FOR VERTICALLY NEIGHBOURING SITES

So far, the results shown for the mixed spin-1 and spin-$\frac{1}{2}$ ladder only had an antiferromagnetic coupling between spins, when $J_0 > 0$ and $J_1 > 0$. A question posed here is how the results showed so far will change as the vertical coupling between sites J_1 becomes ferromagnetic, when J_1 transits to negative values ($J_1 < 0$).

When $J_1 < 0$, the vertically neighboring spins will have an alignment tendency, while horizontal sites will tend to counter-align. This will lead to a different ground state of the Hamiltonian H_0 (figure 33).

Before, all sites had a tendency of counter alignment, since the material was purely antiferromagnetic (but exhibiting a net magnetization, since sites had alternating spin values). It was anticipated that the lowest energy level would correspond to a total S^z of 1 per unit cell and the magnetization curve featured a magnetization plateau. However, the gap size decreased as the value of J_1 got smaller and it can be anticipated that the gap will tend to zero as J_1 gets increasingly negative. In fact, in the limit where $J_1 \to -\infty$, J_1 becomes much greater than J_0 (which would be equivalent to $J_0 \to 0$) and the Hamiltonian gap is observed to be non-existent, as the chain becomes purely ferromagnetic and the Hamiltonian becomes gapless.

Figura 33 – Ground state ordering of the ferromagnetic vertical coupled ladder with antiferromagnetic horizontal coupling ($J_1 < 0$ and $J_0 > 0$). The total magnetization of this state corresponds to 0 per unit cell.

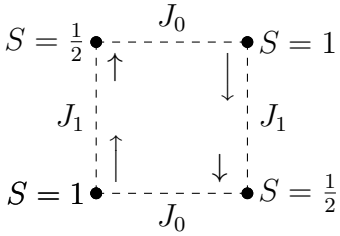

Source: the author (2022).

5.3.1 Energy levels $E_0(S^z)$ and magnetization curve

With $J_1 < 0$, the ground state at zero magnetic field is a singlet, displaying zero magnetization. Again, for this section, the coupling J_0 will be set equal to 1, and J_1 will take multiple

values for the energy levels at zero magnetic field (figure 34) and magnetization as a function of a magnetic field (figure 35). Also, the energy curves no longer present the energy degenerescence at magnetization ranging from 0 to $\frac{1}{3}$ of the saturation value, but it is possible to see that there is a discontinuity on the slope of the curve. However, this discontinuity decreases as J_1 becomes more negative, indicating the gap size is decreasing.

The magnetization per unit cell as a function of the applied magnetic field has many differences when compared to the ferrimagnetic case. The $\frac{1}{3}$-plateau is clearly decreasing its size as J_1 becomes more negative, indicating a phase transition from a gapped to gapless phase. This transition occurs at constant magnetization given by 1 per unit cell, with no symmetry breaks. Such transition consists of a Kosterlitz-Thouless phase transition.

Figura 34 – Mixed spin-1 and spin-$\frac{1}{2}$ ladder energy levels $E_0(S^z)$ with $h_B = 0$ and ferromagnetic vertical coupling. The number of unit cells was $L = 20$, totaling 80 sites.

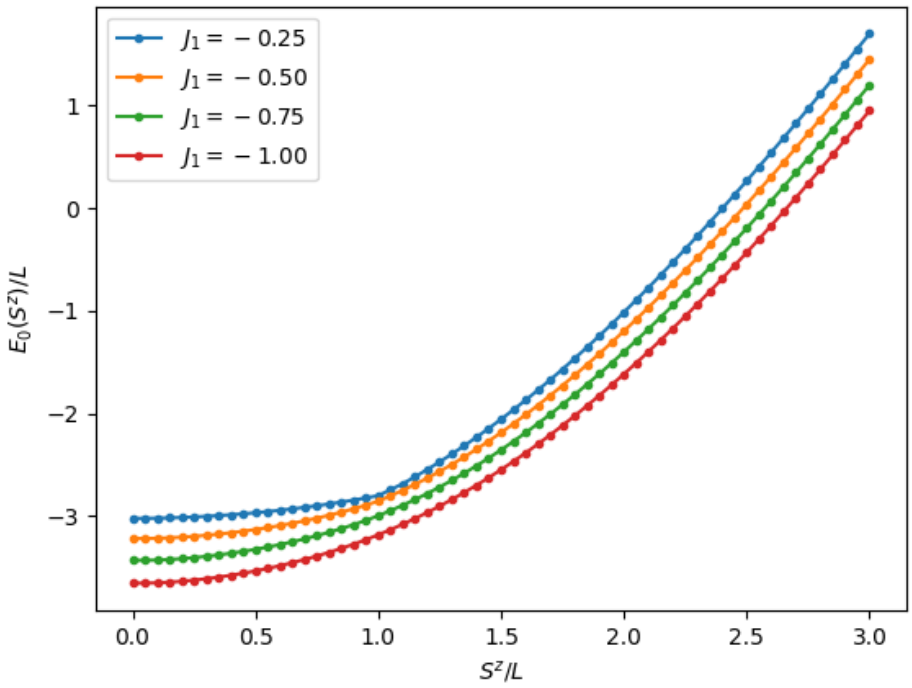

Source: the author (2022).

Figura 35 – Mixed spin ladder magnetization per unit cell as a function of the magnetic field h_B. Number of unit cells $L = 20$, totaling 80 sites. Note the magnetization gap as in the spin one chain case.

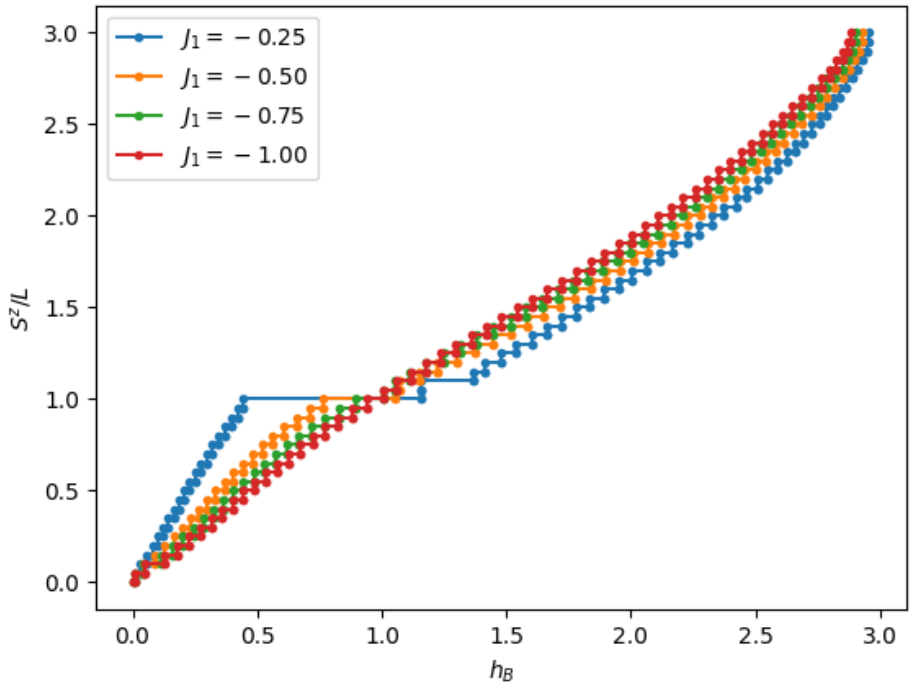

Source: the author (2022).

5.3.2 Spin orientation of the mixed spin ladder with sites spin 1 and $\frac{1}{2}$ with ferromagnetic coupling

The local magnetization along the lattice (figure 36) is structurally different from the one presented in figure 30, although the magnetization levels portrayed are the same ones. One may see that magnetization in the chain's interior remains uniform for all levels, something that did not occur in the ferrimagnetic case. There will be no parallel with free particle confined to a potential well for this case and the wave function will have a completely different format, as can be seen from the difference of local S^z between the total S^z levels (figure 37).

Figura 36 – Alternating ladder with sites spin 1 and $\frac{1}{2}$ dimer spin orientation with ferromagnetic vertical coupling. The number of unit cells was $L = 20$, totaling 80 sites. $J_1 = -J_0 = -1$.

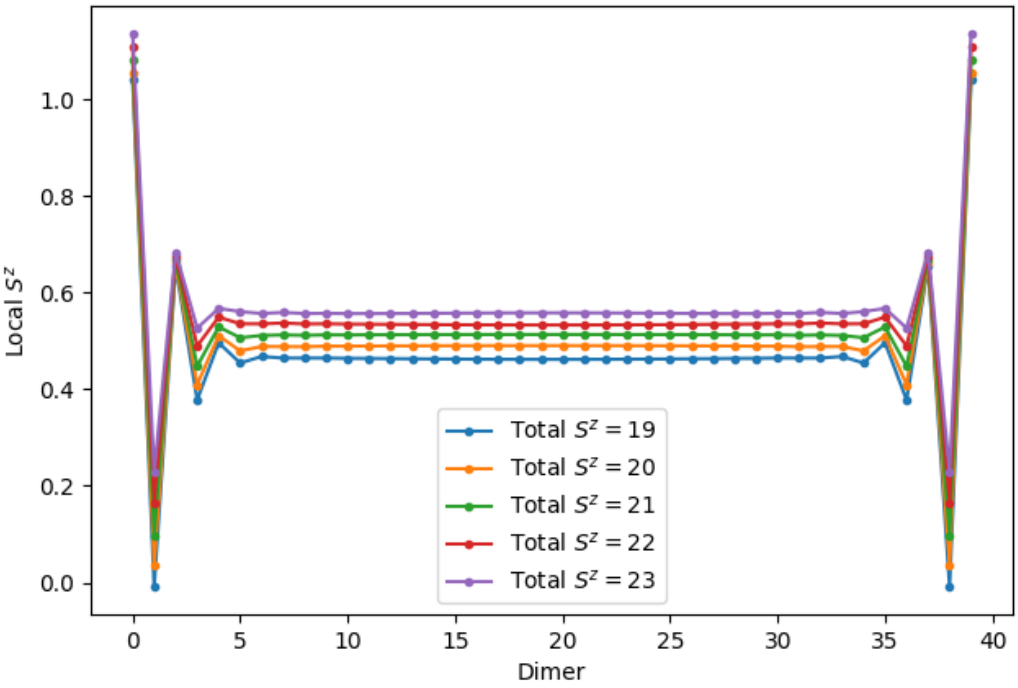

Source: the author (2022).

Figura 37 – Local S^z difference for different total S^z levels. $J_1 = -J_0 = -1$.

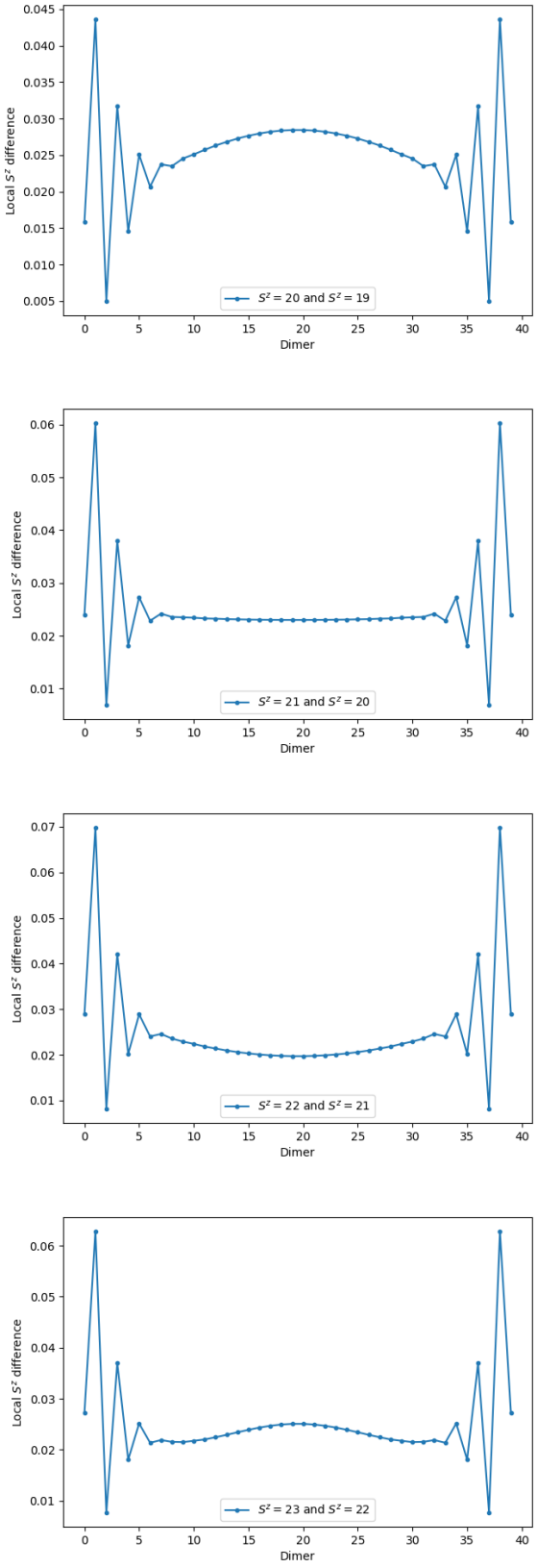

Source: the author (2022).

5.4 SCALE ANALYSIS

The results showed were obtained using fixed sizes of chains in the DMRG numerical procedure. In order to investigate the physical properties in the thermodynamic limit, it is necessary to run the DMRG for multiple chain sizes. It is necessary now to elaborate on how it is possible to extrapolate the data obtained for DMRG runs with multiple chain sizes to the thermodynamic limit.

There are two magnetic field values that must be highlighted in order to define the magnetization plateau size: h_B^- and h_B^+, defined to be the magnetic fields of the beginning and end of the magnetization plateau, respectively. The field h_B^- is the magnetic field that excites the chain into the magnetization plateau, while the field h_B^+ excites the chain to the first level above the magnetization plateau. Then, the magnetization plateau size is simply given by $\Delta H_B = h_B^+ - h_B^-$. These values of fields are obtained using equation (2.25). Since the energy levels are used to obtain both h_B^+ and h_B^-, it is clear that the magnetization plateau size may fluctuate with the chain size. In order to determine the plateau size in the thermodynamic limit, it will be done a data extrapolation to the $L \to \infty$ limit. To accomplish this, it is necessary to study the dependence that the gap length has on the chain size, and then look for a pattern to extrapolate the gap to the thermodynamic limit.

One could plot the gap size as a function of L and try to determine a polynomial to extrapolate the gap size as $L \to \infty$. However, this would possibly lead to complications, since the limit $L \to \infty$ is not convergent. An intuitive alternative would be to plot the gap size as a function of $\frac{1}{L}$, since $\frac{1}{L}$ converges to zero as $L \to \infty$. It will be shown that this approach leads to very good results to extrapolate gap size in the thermodynamic limit, since, usually, the gap size will be a linear function of $\frac{1}{L}$. Then, all that would be necessary to determine the gap size in the thermodynamic limit would be to find the best linear fit for the points and determine the linear function's intercept with the y axis. This is the procedure by which the gaps are determined as a function of the couplings.

Lastly, by assembling data on the dependence of the gaps as functions of the coupling, it is possible to investigate an analytical form of dependence between the gap in the thermodynamic limit and the coupling of the spins. One of the subjects of interest is to determine how the gaps approach zero by varying the spin coupling values.

5.4.1 The $\frac{1}{L}$ dependence

The magnetization plateau size ΔH_B is expected to change for different values of L. Since the gap is expected to converge to some finite value in the thermodynamic limit, the gap size can be written as a series expansion in $\frac{1}{L}$ of the form

$$\Delta H_B = \sum_{n}^{\infty} a_n \left(\frac{1}{L}\right)^n \tag{5.2}$$

Note that, for $L \to \infty$, the series will naturally converge to a finite value, as long as the coefficients are finite. However, it is unnecessary to write the gap size as an infinite sum: it can be fairly accurate to simply use a first-order expansion. The gap size equation then reduces to the simpler form of

$$\Delta H_B = a\frac{1}{L} + b \tag{5.3}$$

Of course, this is only a good approximation if the values of L used are big enough so that higher orders of $\frac{1}{L}$ can be dismissed.

According to equation (5.3), in the thermodynamic limit, the gap size will simply be the intercept value b. The mixed spin-1 and spin-$\frac{1}{2}$ ladder chain have a gap in its magnetization curve that can be seen to decrease as the value of J_1 decreases. For a generic size L, the magnetization plateau starts at total $S^z = 1$ per unit cell. In terms of the chain total S^z, the magnetization will be equal to L. Hence, the field h_B^- will be given by

$$h_B^- = E_0(L) - E_0(L-1).$$

In finite systems, the mixed spin ladder has two magnetization plateaus steps. However, the second step can be seen to be small as the lattice size increases. While the second step represents a magnetization increase, in the thermodynamic limit, this increase becomes insignificant and a very small increase can be interpreted as no increase at all: the magnetization plateau becomes a longer interval at which the magnetization stays constant, with no steps in the middle. The expression for the h_B^+ field is equal to

$$h_B^+ = E_0(L+3) - E_0(L+2).$$

The magnetization plateau size is then given by the difference between h_B^+ and h_B^-, as mentioned before, equal to

$$\Delta H_B = h_B^+ - h_B^- = E_0(L+3) - E_0(L+2) - E_0(L) + E_0(L-1). \tag{5.4}$$

Running the DMRG for multiple values of L and evaluating the gap size, a linear fit can be used to determine the values of a and b. Since the expression for the gap size depends only on the energy levels of states $S^z = L+3$, $L+2$, L, and $L-1$, the DMRG need only to be run at these subspaces of total S^z value. It is expected that a linear fit will be a good approximation for the multiple plot points $(\frac{1}{L}, \Delta H_B)$ obtained running the DMRG.

In order to test the gap convergence in the thermodynamic limit, consider the case in which $J_1 = J_0 = 1$ (figure 38).

Figura 38 – Ferrimagnetic ladder gap size as a function of $\frac{1}{L}$.

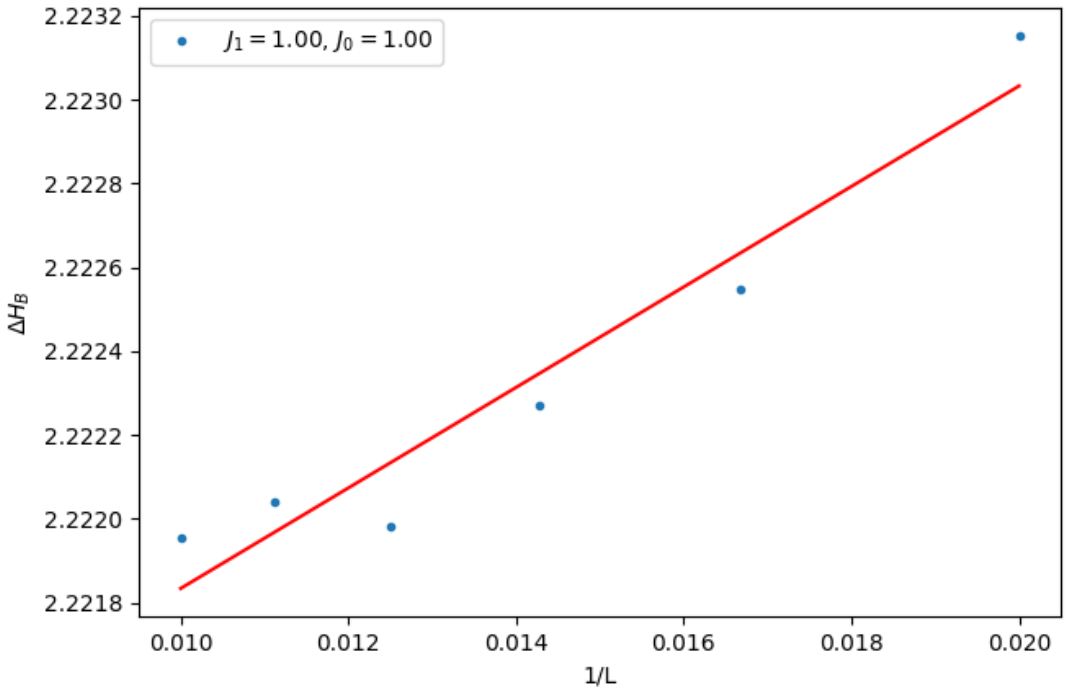

Source: the author (2022).

An important error measurement when performing a linear fit is the total quadratic distance of the points to the linear function ϵ^2. For these points, the linear fit had the value of ϵ^2 given by

$$\epsilon^2 = 7.12112434673 \times 10^{-8},$$

a relatively small value. This serves as an argument to show that the linear fit was a good approximation. Also, the intercept, which is equivalent to the gap size in the thermodynamic limit, had a value of $\Delta H_B = 2.22063615742$, in agreement with the value shown at (LANGARI; MARTÍN-DELGADO, 2000).

At this point, a conclusion can be drawn regarding how to investigate the physical properties of the thermodynamic limit. It is expected that any physical observable will converge to some value in the thermodynamic limit, in which $\frac{1}{L} \to 0$. If appropriate values of L are chosen, there is a possibility of a good linear fit. Else, there are probably gonna be higher order terms of $(1/L)$ in the approximation, such as depicted by equation (5.2). The points that end up falling outside the linear fit are due to energy fluctuations and natural errors that occur in numerical processes.

5.4.2 Ferromagnetic vertical coupling

For negative values of J_1, the linear fit continues to be a good approximation to investigate the gape size in the thermodynamic limit. The $J_1 = -1$ and $J_0 = 1$ (figure 39) case can be seen to have very small error ϵ^2 and the points are well fit by a linear function. It was obtained for the total quadratic error ϵ^2 and gap at thermodynamic limit ΔH_B the following values: $\epsilon^2 = 1.45237663547 \times 10^{-8}$ and $\Delta H_B = 0.00331926049413$. The gap size is considerably smaller. This is due to the coupling J_1 having such a negative value. This leads to yet another investigation: how the system transits from gapped to gapless as J_1 becomes more negative. This will be done by setting J_0 fixed at 1, while J_1 will range from 0 to -1.

Figura 39 – Mixed spin ladder gap size as a function of $\frac{1}{L}$. $J_1 = -1$. J_0 fixed at 1.

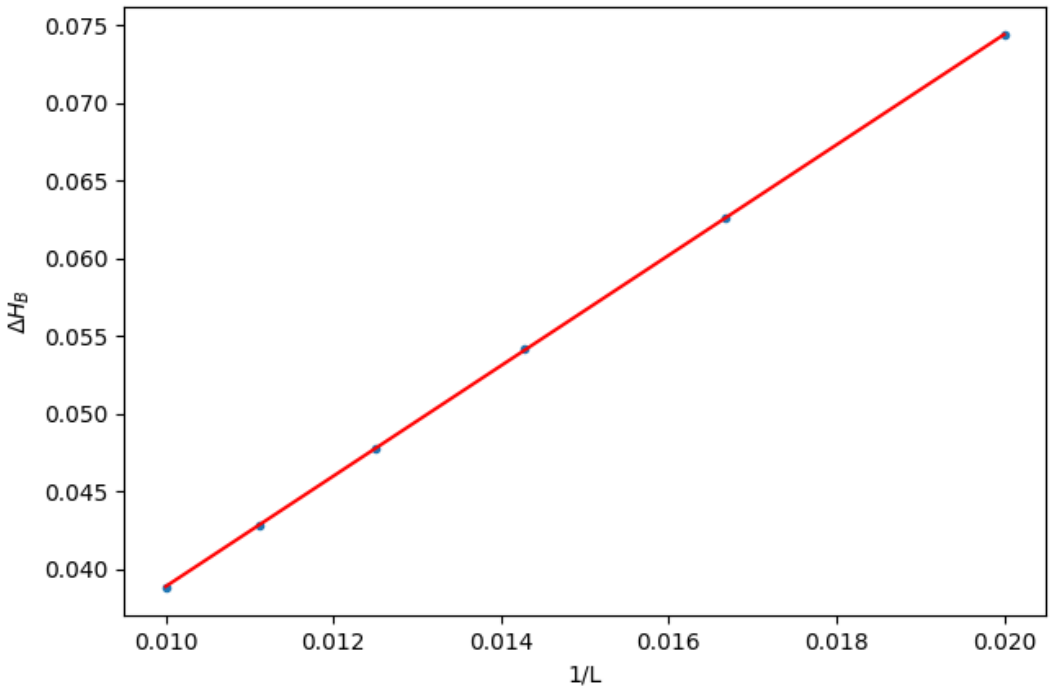

Source: the author (2022).

There are different linear fits for multiple values of J_1, with J_0 fixed at 1. As J_1 tends to $-\infty$, the linear fits will converge to having null intercept (figure 40), which corroborates with the fact the gap is null when $J_0 = 0$ and $J_1 = -1$.

Figura 40 – Mixed spin ladder gap size as a function of $\frac{1}{L}$. Values of J_1 are given by $J_1 = -0.1$, -0.2, -0.3, -0.4, -0.5, -0.6, -0.7, -0.8, -0.9 and -1. J_0 fixed at 1.

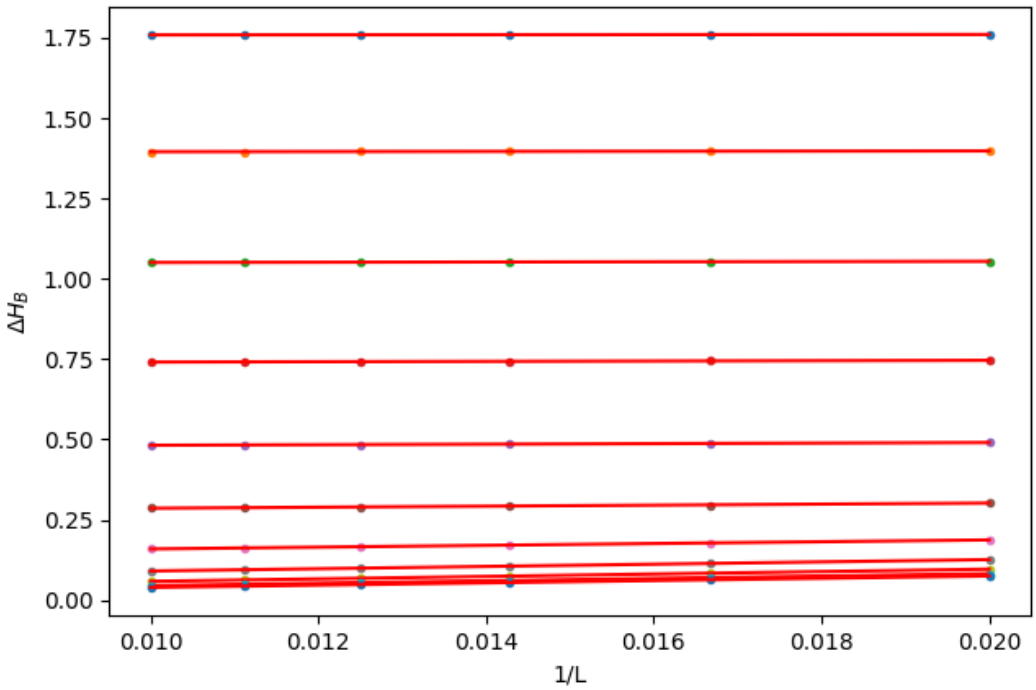

Source: the author (2022).

The gap size in the thermodynamic limit as a function of J_1 with J_0 fixed at 1 has an asymptotic behavior (figure 41). As J_1 approaches the critical value J_c from above, the system will transit from a gapped phase to a gapless phase.

Figura 41 – Mixed spin ladder magnetization plateau size at thermodynamic limit as a function of J_1. J_0 fixed at 1.

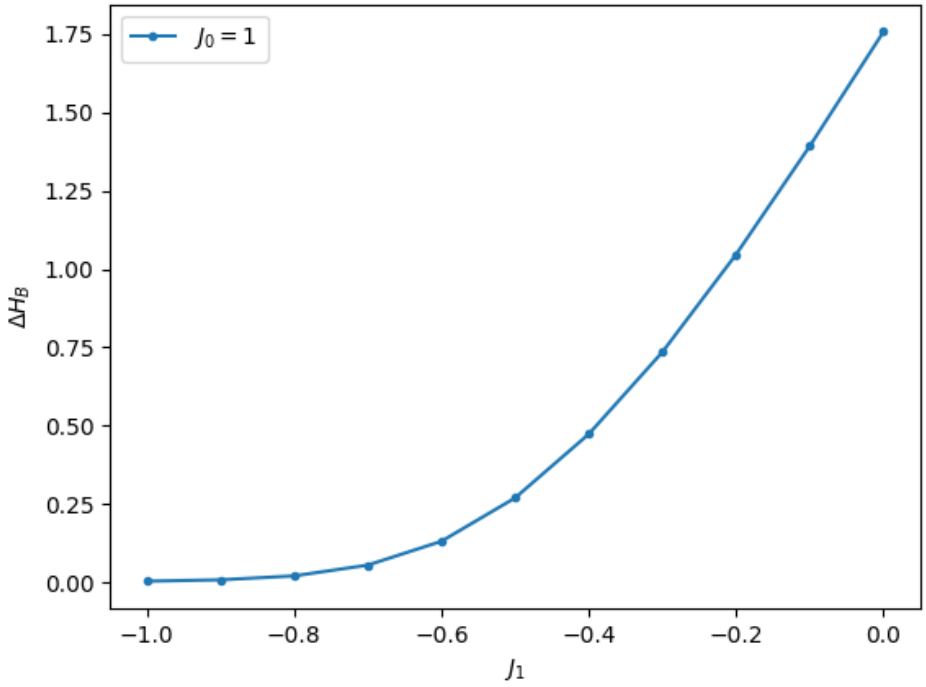

Source: the author (2022).

5.4.3 Critical value J_c, exponential dependency, and Kosterlitz-Thouless phase transition

In order to determine the critical value of J_c using the finite chain size DMRG run, a simple process can be argued. As J_1 approaches the critical value J_c, the plateau size ΔH_B will decrease, no matter what size of L is being used to evaluate the numeric process. For J_1 below the critical value J_c, the Hamiltonian will be gapless. For infinite L, there will be an infinitesimal difference between consecutive energy levels. So, as L increases, the gap ΔH_B will tend to decrease. However, the product $L\Delta H_B$ may remain constant (VERÍSSIMO et al., 2019). At the critical value, it is expected that the product $L\Delta H_B$ will converge to a finite value (figure 42).

Figura 42 – Product $L\Delta H_B$. Note how the product converges as J_1 tends to 1, meaning that J_1 approaches the critical value J_c.

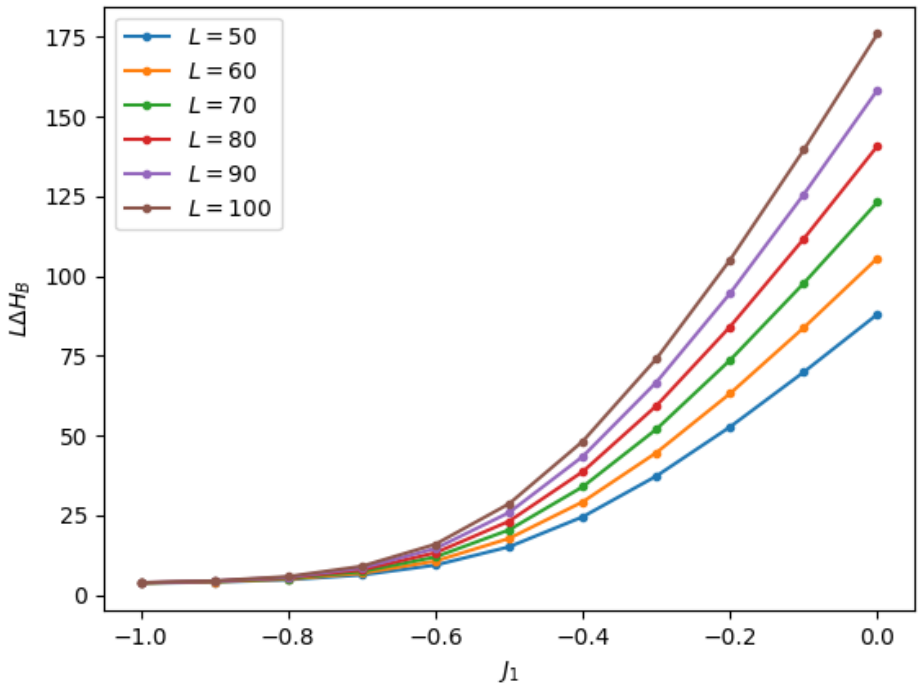

Source: the author (2022).

The gap size with J_1 above the critical value J_c is modeled to have an exponential dependency, with a generic form given by

$$\Delta H_B = Ae^{-b(J_1 - J_c)^{-\gamma}}. \tag{5.5}$$

Here, both b and γ are positive constants. Note that the gap will tend to zero when $J_1 \to J_c^+$.

Taking the natural logarithm in equation (5.5) will lead to

$$\ln \Delta H_B = \ln A - b(J_1 - J_c)^{-\gamma}. \tag{5.6}$$

In order to determine the parameters A, b, γ and J_c, it is necessary to find the linear fit of $\ln \Delta H_B$ as a linear function of $(J_1 - J_c)^{-\gamma}$ that results in the least total quadratic error. J_c and γ are varied in order to find the parameters that have the least total quadratic error.

For $J_c = -1$ and $\gamma = -0.5$, it was possible to obtain a good linear (figure 43) fit, with a small error ϵ^2, given by $\epsilon^2 = 5.92926854277065 \times 10^{-4}$. In the thermodynamic limit, when J_1 reaches the critical value of J_c, there will be a phase transition, as the system will transit from

a gapped to a gapless phase. The exponential dependence of the gap takes the same form as a Kosterlitz-Thouless phase transition.

The phase diagram (figure 44) will contain gapped phases (the $\frac{1}{3}$-plateau), gapless phases (Luttinger liquid phase), and a Kosterlitz-Thouless phase transition.

Figura 43 – Natural logarithm of the gap in the thermodynamic limit $\ln \Delta H_B$ as a function of $(J_1 - J_c)^{-0.5}$, with $J_c = -1$.

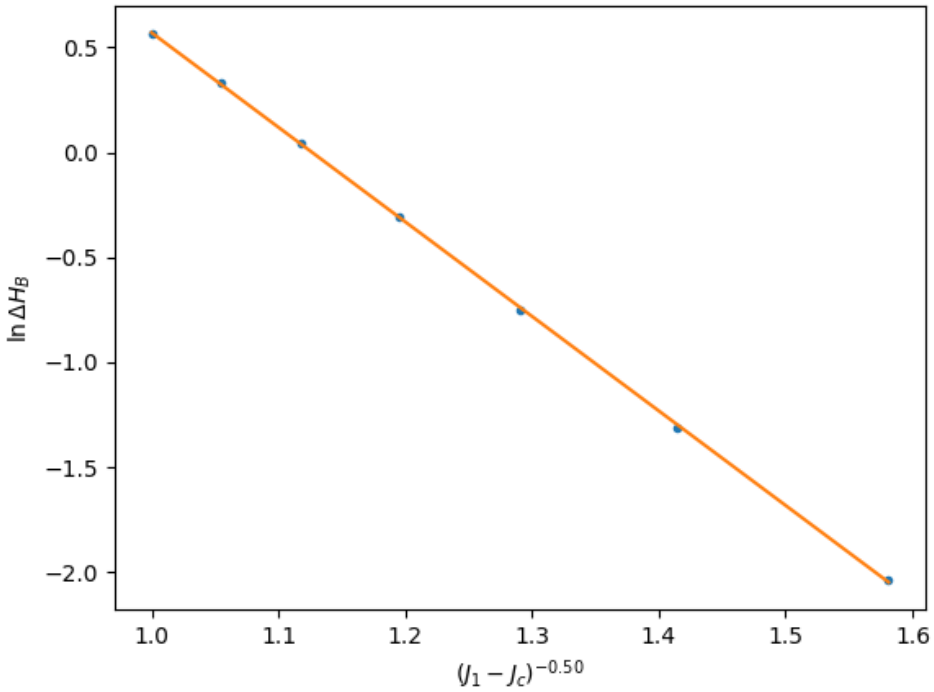

Source: the author (2022).

Figura 44 – Magnetic field vs coupling parameter phase diagram of the mixed spin-1 and spin-$\frac{1}{2}$ ladder.

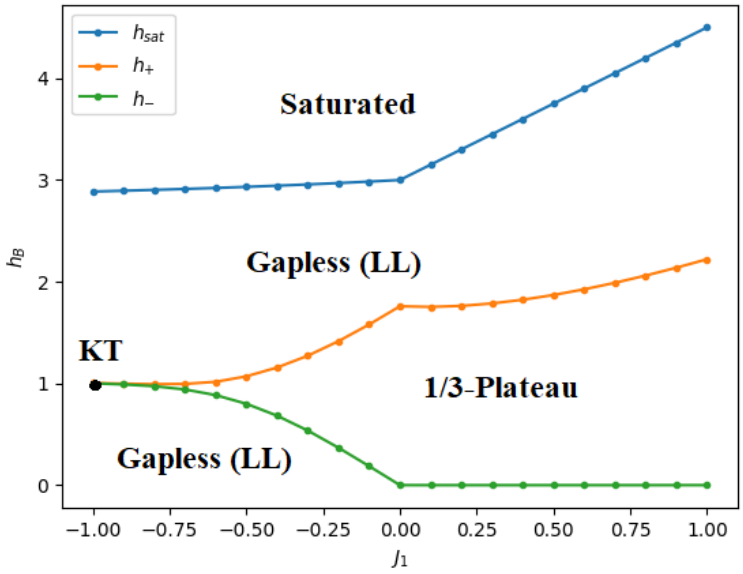

Source: the author (2022).

6 CONCLUSION

Quantum phase transitions were investigated for multiple spin models described by the Heisenberg Hamiltonian. Using the DMRG to determine the energy levels of the Hamiltonian at zero magnetic field, it was observed that some chains have gapped energy levels, which leads to magnetization plateaus in the magnetization curve. By applying a magnetic field, it is possible to observe transitions from gapped to gapless phases. That was the case of the antiferromagnetic spin-1 chain, the antiferromagnetic spin-$\frac{1}{2}$ ladder, and the antiferromagnetic mixed spin-1 and spin-$\frac{1}{2}$ chain.

For the mixed spin-1 and spin-$\frac{1}{2}$ ladder, the gap size depends on the chain's spin-coupling J_1 and J_0. It was observed that for antiferromagnetic coupling ($J_0 > 0$ and $J_1 > 0$), the ground state is gapped and the magnetization curve has a plateau at magnetization given by $\frac{1}{3}$ of the saturation value, the $\frac{1}{3}$-plateau.

Another form to obtain the transition from gapped to gapless phases is achieved by varying the spin-coupling. With J_0 fixed at 1 and $J_1 < 0$, the ground state at zero magnetic field is a singlet and gapless. However, the system still exhibits the $\frac{1}{3}$-plateau depending on the value of J_1. It is observed that the plateau size decreases as J_1 approaches a critical value J_c. With finite scale analysis, it was possible to extrapolate the plateau size to the thermodynamic limit using the DMRG data obtained with finite-size chains, and it was determined that the system would have a transition to a gapless phase at $J_1 = -1$.

The phase transition occurs with no symmetry breaking since magnetization remains constant in this transition. Because of it, the transition is a Kosterlitz-Thouless phase transition, and the plateau size will have an exponential dependence. The applied magnetic field versus coupling J_1 phase diagram contains a saturated phase (when magnetization reaches the maximum value), gapless phases (Luttinger liquid), a gapped phase ($\frac{1}{3}$-plateau) and a Kosterlitz-Thouless phase transition point. The lines represent second-order phase transitions.

REFERENCES

AFFLECK, I. Quantum spin chains and the Haldane gap. *Journal of Physics: Condensed Matter*, v. 1, p. 3047–3072, 5 1989. ISSN 0953-8984. Available at: <https://iopscience.iop.org/article/10.1088/0953-8984/1/19/001>.

AFFLECK, I. Theory of Haldane-gap antiferromagnets in applied fields. *Physical Review B*, v. 41, p. 6697–6702, 4 1990. ISSN 0163-1829. Available at: <https://link.aps.org/doi/10.1103/PhysRevB.41.6697>.

AFFLECK, I.; LIEB, E. H. A proof of part of Haldane's conjecture on spin chains. *Letters in Mathematical Physics*, v. 12, p. 57–69, 7 1986. ISSN 0377-9017. Available at: <http://link.springer.com/10.1007/BF00400304>.

AZUMA, M.; HIROI, Z.; TAKANO, M.; ISHIDA, K.; KITAOKA, Y. Observation of a spin gap in $SrCu_2O_3$ comprising spin- quasi-1d two-leg ladders. *Physical Review Letters*, v. 73, p. 3463–3466, 12 1994. ISSN 00319007. Available at: <https://link.aps.org/doi/10.1103/PhysRevLett.73.3463>.

BARNES, T.; DAGOTTO, E.; RIERA, J.; SWANSON, E. S. Excitation spectrum of Heisenberg spin ladders. *Physical Review B*, v. 47, p. 3196–3203, 2 1993. ISSN 0163-1829. Available at: <https://link.aps.org/doi/10.1103/PhysRevB.47.3196>.

BAUER, B.; CARR, L. D.; EVERTZ, H. G.; FEIGUIN, A.; FREIRE, J.; FUCHS, S.; GAMPER, L.; GUKELBERGER, J.; GULL, E.; GUERTLER, S.; HEHN, A.; IGARASHI, R.; ISAKOV, S. V.; KOOP, D.; MA, P. N.; MATES, P.; MATSUO, H.; PARCOLLET, O.; PAWŁOWSKI, G.; PICON, J. D.; POLLET, L.; SANTOS, E.; SCAROLA, V. W.; SCHOLLWÖCK, U.; SILVA, C.; SURER, B.; TODO, S.; TREBST, S.; TROYER, M.; WALL, M. L.; WERNER, P.; WESSEL, S. The alps project release 2.0: open source software for strongly correlated systems. *Journal of Statistical Mechanics: Theory and Experiment*, v. 2011, p. P05001, 5 2011. ISSN 1742-5468. Available at: <https://iopscience.iop.org/article/10.1088/1742-5468/2011/05/P05001>.

BREHMER, S.; MIKESKA, H.-J.; YAMAMOTO, S. Low-temperature properties of quantum antiferromagnetic chains with alternating spins $s = 1$ and $s = 1/2$. *Journal of Physics: Condensed Matter*, v. 9, p. 3921–3930, 5 1997. ISSN 0953-8984. Available at: <https://iopscience.iop.org/article/10.1088/0953-8984/9/19/012>.

CONTINENTINO, M. A. Topological phase transitions. *Physica B: Condensed Matter*, v. 505, p. A1–A2, 1 2017. ISSN 09214526. Available at: <https://linkinghub.elsevier.com/retrieve/pii/S0921452616305117>.

COUTINHO-FILHO, M. D.; MONTENEGRO-FILHO, R. R.; RAPOSO, E. P.; VITORIANO, C.; OLIVEIRA, M. H. Magnetism and electronic correlations in quasi-one-dimensional compounds. *Journal of the Brazilian Chemical Society*, v. 19, p. 232–244, 2008. ISSN 0103-5053. Available at: <https://www.scielo.br/j/jbchs/a/4dB6kjybfNWKmQSrrsCWj6G/?lang=en>.

DAGOTTO, E.; RICE, T. M. Surprises on the way from one- to two-dimensional quantum magnets: The ladder materials. *Science*, v. 271, p. 618–623, 2 1996. ISSN 0036-8075. Available at: <https://www.science.org/doi/10.1126/science.271.5249.618>.

FRICKE, T. Monte Carlo investigation of the Ising model. *Ohio state university*, 2006. Available at: <https://www.asc.ohio-state.edu/braaten.1/statphys/Ising_MatLab.pdf>.

GIAMARCHI, T.; RÜEGG, C.; TCHERNYSHYOV, O. Bose–Einstein condensation in magnetic insulators. *Nature Physics*, v. 4, p. 198–204, 3 2008. ISSN 1745-2473. Available at: <http://www.nature.com/articles/nphys893>.

HALDANE, F. Continuum dynamics of the 1-d Heisenberg antiferromagnet: Identification with the o(3) nonlinear sigma model. *Physics Letters A*, v. 93, p. 464–468, 2 1983. ISSN 03759601. Available at: <https://linkinghub.elsevier.com/retrieve/pii/037596018390631X>.

HALDANE, F. D. M. Nonlinear field theory of large-spin Heisenberg antiferromagnets: Semiclassically quantized solitons of the one-dimensional easy-axis Néel state. *Physical Review Letters*, v. 50, p. 1153–1156, 4 1983. ISSN 0031-9007. Available at: <https://link.aps.org/doi/10.1103/PhysRevLett.50.1153>.

HOHENBERG, P. C. Existence of long-range order in one and two dimensions. *Physical Review*, v. 158, p. 383–386, 6 1967. ISSN 0031-899X. Available at: <https://link.aps.org/doi/10.1103/PhysRev.158.383>.

ISHIDA, K.; KITAOKA, Y.; ASAYAMA, K.; AZUMA, M.; HIROI, Z.; TAKANO, M. Spin gap behavior in ladder-type of quasi-one-dimensional spin (s=1/2) system $SrCu_2O_3$. *Journal of the Physical Society of Japan*, v. 63, p. 3222–3225, 9 1994. ISSN 13474073. Available at: <http://journals.jps.jp/doi/10.1143/JPSJ.63.3222>.

IVANOV, N. B. Spin models of quasi-1d quantum ferrimagnets with competing interactions. *Condensed Matter Physics*, v. 12, p. 435–447, 2009. ISSN 1607324X. Available at: <http://www.icmp.lviv.ua/journal/zbirnyk.59/010/abstract.html>.

JOHNSTON, D. C.; JOHNSON, J. W.; GOSHORN, D. P.; JACOBSON, A. J. Magnetic susceptibility of $(VO)_2P_2O_7$: A one-dimensional spin-1/2 Heisenberg antiferromagnet with a ladder spin configuration and a singlet ground state. *Physical Review B*, v. 35, p. 219–222, 1987. ISSN 01631829. Available at: <https://journals.aps.org/prb/abstract/10.1103/PhysRevB.35.219>.

JOLICOEUR, T.; GOLINELLI, O. Physics of integer-spin antiferromagnetic chains: Haldane gaps and edge states. *Comptes Rendus Chimie*, v. 22, p. 445–451, 6 2019. ISSN 16310748. Available at: <https://linkinghub.elsevier.com/retrieve/pii/S1631074819300943>.

KOBE, S. Ernst Ising 1900-1998. *Brazilian Journal of Physics*, v. 30, p. 649–654, 12 2000. ISSN 0103-9733. Available at: <https://www.scielo.br/j/bjp/a/7psskCZXtFRmYs6fGRrjYkJ/?lang=en>.

KOLEZHUK, A. K.; MIKESKA, H.-J.; YAMAMOTO, S. Matrix-product-states approach to Heisenberg ferrimagnetic spin chains. *Physical Review B*, v. 55, p. R3336–R3339, 2 1997. ISSN 0163-1829. Available at: <https://link.aps.org/doi/10.1103/PhysRevB.55.R3336>.

KONG, L. B.; LIU, L.; YANG, Z.; LI, S.; ZHANG, T.; WANG, C. *Theory of ferrimagnetism and ferrimagnetic metal oxides*. Elsevier, 2018. 287-311 p. Available at: <https://linkinghub.elsevier.com/retrieve/pii/B9780128111802000153>.

KOSTERLITZ, J. M. The critical properties of the two-dimensional xy model. *Journal of Physics C: Solid State Physics*, v. 7, p. 1046–1060, 3 1974. ISSN 0022-3719. Available at: <https://iopscience.iop.org/article/10.1088/0022-3719/7/6/005>.

KOSTERLITZ, J. M.; THOULESS, D. J. Ordering, metastability and phase transitions in two-dimensional systems. *Journal of Physics C: Solid State Physics*, v. 6, p. 1181–1203, 4 1973. ISSN 0022-3719. Available at: <https://iopscience.iop.org/article/10.1088/0022-3719/6/7/010>.

LANGARI, A.; MARTÍN-DELGADO, M. A. Alternating-spin ladders in a magnetic field: Formation of magnetization plateaus. *Physical Review B*, v. 62, p. 11725–11730, 11 2000. ISSN 0163-1829. Available at: <https://link.aps.org/doi/10.1103/PhysRevB.62.11725>.

LIEB, E.; MATTIS, D. Ordering energy levels of interacting spin systems. *Journal of Mathematical Physics*, v. 3, p. 749–751, 7 1962. ISSN 0022-2488. Available at: <http://aip.scitation.org/doi/10.1063/1.1724276>.

MAISINGER, K.; SCHOLLWÖCK, U.; BREHMER, S.; MIKESKA, H. Thermodynamics of the ferrimagnet in finite magnetic fields. *Physical Review B - Condensed Matter and Materials Physics*, v. 58, p. R5908–R5911, 9 1998. ISSN 1550235X. Available at: <https://link.aps.org/doi/10.1103/PhysRevB.58.R5908>.

MALVEZZI, A. L. An introduction to numerical methods in low-dimensional quantum systems. *Brazilian Journal of Physics*, v. 33, 3 2003. ISSN 0103-9733. Available at: <https://www.scielo.br/j/bjp/a/yTTksYZLSycW8tm9MJ3vG3h/?lang=en>.

MERMIN, N. D.; WAGNER, H. Absence of ferromagnetism or antiferromagnetism in one- or two-dimensional isotropic Heisenberg models. *Physical Review Letters*, v. 17, p. 1133–1136, 11 1966. ISSN 0031-9007. Available at: <https://link.aps.org/doi/10.1103/PhysRevLett.17.1133>.

MONTENEGRO-FILHO, R. R.; MATIAS, F. S.; COUTINHO-FILHO, M. D. Topology of many-body edge and extended quantum states in an open spin chain: 1/3 plateau, Kosterlitz-Thouless transition, and Luttinger liquid. *Physical Review B*, v. 102, p. 035137, 7 2020. ISSN 2469-9950. Available at: <https://link.aps.org/doi/10.1103/PhysRevB.102.035137>.

MONTENEGRO-FILHO, R. R.; SILVA-JÚNIOR, E. J. P.; COUTINHO-FILHO, M. D. Ground-state phase diagram and thermodynamics of coupled trimer chains. *Physical Review B*, American Physical Society (APS), v. 105, n. 13, p. 134423–1,134423–10, apr 2022. Available at: <https://journals.aps.org/prb/abstract/10.1103/PhysRevB.105.134423>.

OHKAWA, F. J. Temperature dependence of electrical resistivity of metals. *Journal of the Physical Society of Japan*, v. 44, p. 1105–1111, 4 1978. ISSN 0031-9015. Available at: <https://journals.jps.jp/doi/10.1143/JPSJ.44.1105>.

OSHIKAWA, M.; YAMANAKA, M.; AFFLECK, I. Magnetization plateaus in spin chains: "Haldane gap" for half-integer spins. *Phys. Rev. Lett.*, American Physical Society, v. 78, p. 1984–1987, Mar 1997. Available at: <https://link.aps.org/doi/10.1103/PhysRevLett.78.1984>.

O'DONNELL, K. P.; CHEN, X. Temperature dependence of semiconductor band gaps. *Applied Physics Letters*, v. 58, p. 2924–2926, 6 1991. ISSN 0003-6951. Available at: <http://aip.scitation.org/doi/10.1063/1.104723>.

PATI, S. K.; RAMASESHA, S.; SEN, D. Low-lying excited states and low-temperature properties of an alternating spin-1–spin-1/2 chain: A density-matrix renormalization-group study. *Physical Review B*, v. 55, p. 8894–8904, 4 1997. ISSN 0163-1829. Available at: <https://link.aps.org/doi/10.1103/PhysRevB.55.8894>.

PINNEY, M. M.; MOKHTARI, D. A.; AKIVA, E.; YABUKARSKI, F.; SANCHEZ, D. M.; LIANG, R.; DOUKOV, T.; MARTINEZ, T. J.; BABBITT, P. C.; HERSCHLAG, D. Parallel molecular mechanisms for enzyme temperature adaptation. *Science*, v. 371, 3 2021. ISSN 0036-8075. Available at: <https://www.science.org/doi/10.1126/science.aay2784>.

RÜEGG, C.; CAVADINI, N.; FURRER, A.; GÜDEL, H.-U.; KRÄMER, K.; MUTKA, H.; WILDES, A.; HABICHT, K.; VORDERWISCH, P. Bose–Einstein condensation of the triplet states in the magnetic insulator tlcucl3. *Nature*, v. 423, p. 62–65, 5 2003. ISSN 0028-0836. Available at: <http://www.nature.com/articles/nature01617>.

RÜEGG, C.; KIEFER, K.; THIELEMANN, B.; MCMORROW, D. F.; ZAPF, V.; NORMAND, B.; ZVONAREV, M. B.; BOUILLOT, P.; KOLLATH, C.; GIAMARCHI, T.; CAPPONI, S.; POILBLANC, D.; BINER, D.; KRÄMER, K. W. Thermodynamics of the spin Luttinger liquid in a model ladder material. *Physical Review Letters*, v. 101, p. 247202, 12 2008. ISSN 0031-9007. Available at: <https://link.aps.org/doi/10.1103/PhysRevLett.101.247202>.

SACHDEV, S. *Quantum Phase Transitions*. Cambridge University Press, 2011. ISBN 9780521514682. Available at: <https://www.cambridge.org/core/product/identifier/9780511973765/type/book>.

SACHDEV, S.; KEIMER, B. Quantum criticality. *Physics Today*, v. 64, p. 29–35, 2 2011. ISSN 0031-9228. Available at: <http://physicstoday.scitation.org/doi/10.1063/1.3554314>.

SCHOLLWÖCK, U. The density-matrix renormalization group. *Reviews of Modern Physics*, American Physical Society, v. 77, p. 259–315, 4 2005. ISSN 0034-6861. Available at: <https://link.aps.org/doi/10.1103/RevModPhys.77.259>.

SILVA, W. M. d. *Teoria de ondas de spin para ferrimagnetos (s, S) com campo magnético aplicado*. Phd Thesis (PhD Thesis) — Universidade Federal de Pernambuco, 2019. Available at: <https://repositorio.ufpe.br/handle/123456789/34288>.

SILVA, W. M. da; MONTENEGRO-FILHO, R. R. Role of density-dependent magnon hopping and magnon-magnon repulsion in ferrimagnetic spin-(1/2, s) chains in a magnetic field. *Physical Review B*, v. 103, p. 054432, 2 2021. ISSN 2469-9950. Available at: <https://link.aps.org/doi/10.1103/PhysRevB.103.054432>.

TENÓRIO, A. S. F.; MONTENEGRO-FILHO, R. R.; COUTINHO-FILHO, M. D. Quantum phase transitions in alternating spin-($\frac{1}{2}$, $\frac{5}{2}$) Heisenberg chains. *Journal of Physics: Condensed Matter*, v. 23, p. 506003, 12 2011. ISSN 0953-8984. Available at: <https://iopscience.iop.org/article/10.1088/0953-8984/23/50/506003>.

VERDAGUER, M.; GLEIZES, A.; RENARD, J. P.; SEIDEN, J. Susceptibility and magnetization of $CuMn(S_2C_2O_2)27.5H_2O$. first experimental and theoretical characterization of a quasi-one-dimensional ferrimagnetic chain. *Physical Review B*, v. 29, p. 5144–5155, 1984. ISSN 01631829. Available at: <https://journals.aps.org/prb/abstract/10.1103/PhysRevB.29.5144>.

VERÍSSIMO, L. M.; PEREIRA, M. S. S.; STREČKA, J.; LYRA, M. L. Kosterlitz-Thouless and Gaussian criticalities in a mixed spin-(1/2, 5/2, 1/2) Heisenberg branched chain with exchange anisotropy. *Physical Review B*, v. 99, p. 134408, 4 2019. ISSN 2469-9950. Available at: <https://link.aps.org/doi/10.1103/PhysRevB.99.134408>.

WAMER, K.; LAJKÓ, M.; MILA, F.; AFFLECK, I. Generalization of the Haldane conjecture to SU(n) chains. *Nuclear Physics B*, v. 952, p. 114932, 3 2020. ISSN 05503213. Available at: <https://linkinghub.elsevier.com/retrieve/pii/S0550321320300183>.

WANG, X.; YU, L. Magnetic-field effects on two-leg Heisenberg antiferromagnetic ladders: Thermodynamic properties. *Physical Review Letters*, v. 84, p. 5399–5402, 6 2000. ISSN 0031-9007. Available at: <https://link.aps.org/doi/10.1103/PhysRevLett.84.5399>.

WHITE, S. R. Density matrix formulation for quantum renormalization groups. *Physical Review Letters*, v. 69, p. 2863–2866, 11 1992. ISSN 0031-9007. Available at: <https://link.aps.org/doi/10.1103/PhysRevLett.69.2863>.

WHITE, S. R. Density-matrix algorithms for quantum renormalization groups. *Physical Review B*, v. 48, p. 10345–10356, 10 1993. ISSN 0163-1829. Available at: <https://link.aps.org/doi/10.1103/PhysRevB.48.10345>.

WHITE, S. R.; NOACK, R. M.; SCALAPINO, D. J. Resonating valence bond theory of coupled Heisenberg chains. *Physical Review Letters*, v. 73, p. 886–889, 8 1994. ISSN 0031-9007. Available at: <https://link.aps.org/doi/10.1103/PhysRevLett.73.886>.

ZHENG, B.; SCHULZ, M.; TRIMPER, S. Dynamic simulations of the Kosterlitz-Thouless phase transition. *Physical Review E*, v. 59, p. R1351–R1354, 2 1999. ISSN 1063-651X. Available at: <https://link.aps.org/doi/10.1103/PhysRevE.59.R1351>.